Bachelorthesis

A Setup for Heterodyne Single-Photon Phase Shift Detection

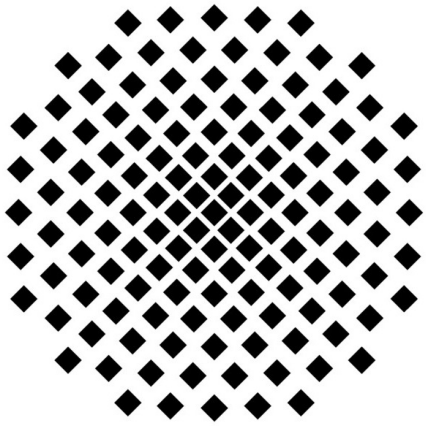

University of Stuttgart

Marian Rockenhäuser

Matrikelnummer: 2875084

Prof Dr. Tilman Pfau
Dr. Sebastian Hofferberth
5. Physikalisches Institut

26.August 2016

Summary

Deutsch

Im Rahmen dieser Bachelorarbeit wurde ein Aufbau zur Messung eines Phasenschubes auf Einzelphotonenbasis realisiert. Dazu wurde ein optisches Interferometer mit einem elektrooptischen Modulator zur Verschiebung der Signalphase aufgebaut. Dabei konnte ein Phasenschub von $1.4\,\pi$ erreicht werden.
Einerseits wurde ein als klassisches Licht anzusehendes Signal, andererseits ein Einzelphotonensignal (Leistung:$1 \cdot 10^{-9}$W) gemessen. Diese wurden mit einer Wechselstromphotodiode (klassisch) und einem Einzel-Photonen-Zähler-Modul (quantisiert) detektiert.
In dieser Bachelorarbeit wird zunächst der notwendige Aufbau mit den verwendeten Geräten besprochen. Gefolgt von einer theoretischen Betrachtung der unterschiedlichen Lichttheorien und deren experimentelle Umsetzung und deren Messergebnissen. Dabei konnte erfolgreich der Phasenschub des Einzelphotonensignal bestimmt werden, sodass das Setup zur Messung eines Phasenschub durch eine Rydbergblockade genutzt werden kann.

English

During this bachelor thesis a setup for a phase shift determination, which is applicable down to a single-photon level were realised. The phase shift on a ligth field, normally imprinted by an atomic blockade, is simulated through a electro-optical modulator. The setup can produce a phase shift of up to $1.4\,\pi$.
On the one hand a high intensity signal, which obeys the classical theory of light and on the other hand a signal on a single-photon level was measured. Therefore, an alternative current photodiode to measure the classical signal and a single photon counter module to measure the single-photon signal was used. To confirm the correctness of the different measurement methods they were compared with each other.
This bachelor thesis reviews the required devices and discusses the implementation of the setup. It is followed by a theoretical consideration of the different light theories and there experimental implementations. Moreover, the results of the measurements are analysed and reviewed in detail.

Declaration

I hereby declare that this submission is my own work and that, to the best of my knowledge and belief, it contains no material previously published or written by another person, except where due acknowledgment has been made in the text.

Marian Rockenhäuser
Stuttgart,26.09.2016

Contents

1 Introduction

In the next ten years computers with standard data transfer via electric impulses are going to reach a performance limit. Those computers are constructed with dissipative logic gates with two states: zero or none. Nonetheless, it is not necessary to realize the logical primitives of a computer with dissipative elements[1]. Through the advent of quantum information processing (QIP) the states are not limited to solely zeros and ones. This could speed up the performance of computers exponentially[2]. To this purpose photons are interesting as carries of quantum information, which can be transmitted easily over long distances, because they hardly interact with their environment. As the central building block of a universal QIP a deterministic photon-photon gate could be used. This would be possible if a single photon light pulse imprints a π phase shift onto a target light pulse [1]. However, because optical photons do not directly interact with each other this leads to difficulties, which could be re-solved by interfacing photons in a medium with an extremely high nonlinearity while preserving optical coherence. A physical mechanism, which can reach such a high nonlinearity is hard to find. Yet, there are a couple of possible strategies to reach the goal of a π phase shift. Fushman showed that a single quantum dot coupled to a photonic crystal can yield a phase shift up to $\pi/4$[3]. Other researchers coupled an optical resonator to an atom or an atomic ensemble [4, 5]. Another possibility is the use of electromagnetically induced transparency (EIT) with low-lying atomic states[6]. Very recently, by using EIT a much smaller phase but conditional cross-phase modulation of 18 μrad was achieved. This result is still several orders of magnitude away from the goal of a π phase shift. However, a promising implementation is the combination of EIT with Rydberg states[7–9]. With this combination an effective phase shift per photon between $\pi/10$ and $\pi/3$ could be reached. So far, only one experiment [10] reached this goal of π. The experiments by Volz[10] and Firstenberg[11] measured the self-phase modulation of a single continuous wave (CW) light field. The other experiments [3, 4] measured the cross-phase modulation (XPM). The XPM was created by one CW light field for another CW light field, but with the extension down to a single photon level the characteristic time of the nonlinearity was too short to spectrally separate the two modes in the XPM. Due to a no-go theorem [12, 13] it should be impossible to achieve an optical QIP on this basis. Therefore, none of these experiments could fulfil the requirement for deterministic optical QIP, where one single photon light field controls another light field. Recently, two experiments used an exception of Shapiro's no-go theorem to create a giant optical Kerr effect. They coherently stored a weak light pulse in an atomic quantum memory via EIT, while sending another light pulse through the EIT medium[14, 15]. These experiments achieved a controlled phase shift of 3.3 rad and π. The setup is similar to the setup of an optical transistor which was a recent experiment of our group[9]. To measure the controlled phase shift, imprinted on the target pulse phase, it is necessary to build a heterodyne single-photon interferometer. In this thesis, a single-photon interferometer was set up and characterized for a later integration in the main experiment.

2 Setup

In this thesis the setup for a measurement of a single photon phase shift was realised. For the measurement of a photon phase shift and its verification by comparing the photon signal with the classical signal an interferometer with two detectors was built.

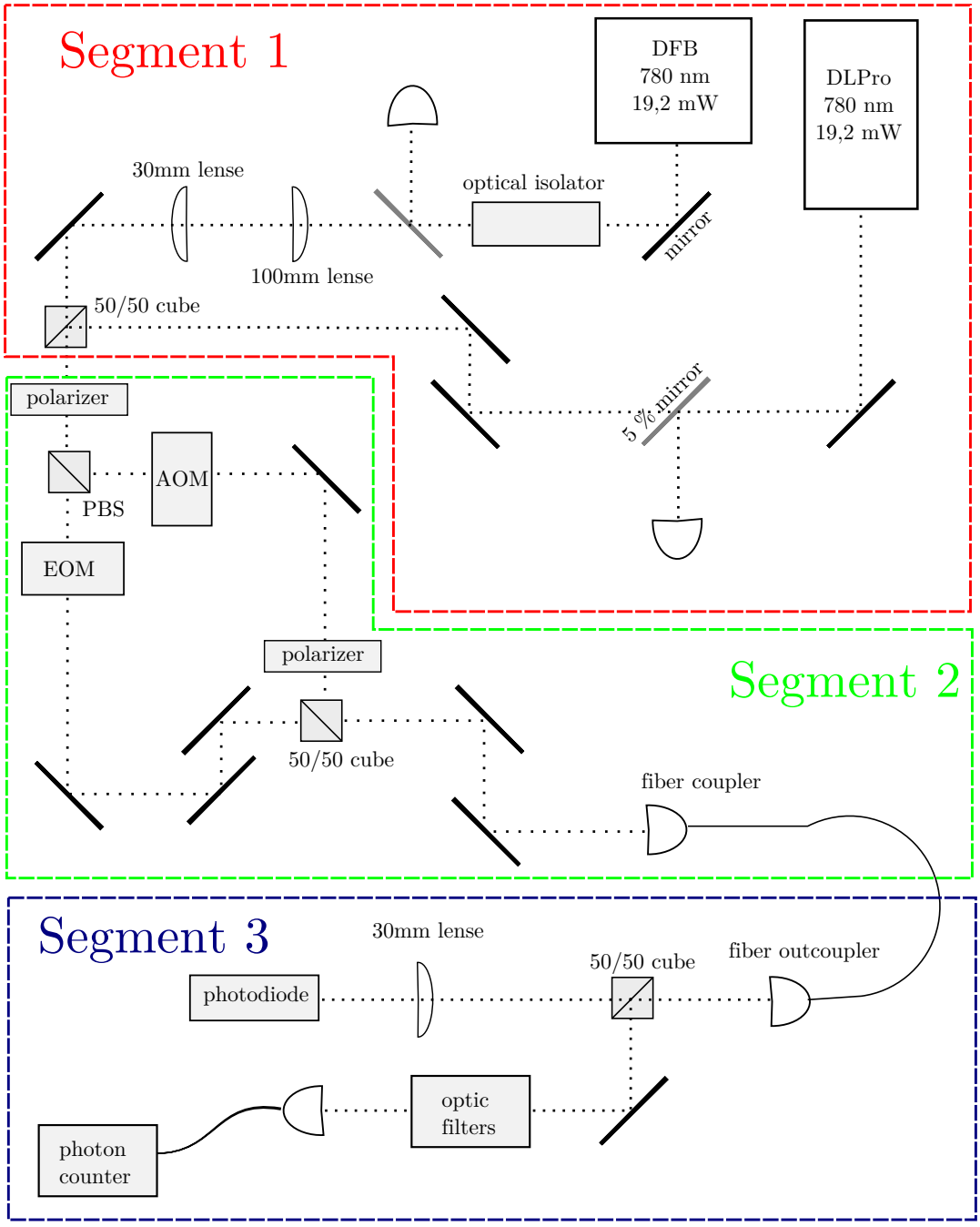

Figure 1: General setup of the few photon interferometer. The setup can be divided in three sections. Segment 1 - Laser Sources, Segment 2 - Interfero-meter and Segment 3 - Detection

The setup can be divided into three segments (see fig.1). In the **first segment** the laser sources are adapted, such that they have the same beam properties. The **second segment** consists of an interferometer with two arms. One arm is modulated with a constant frequency. While the other arm allows the phase to be shifted. Subsequently, the two beam paths are overlapped again to produce interference. The **third segment** is where the measurement takes place in two different ways: the classical signal is detected with a photodiode and the few photon-signal is detected with a photon-counter module.In the following, the requirements for this setup are clarified and the experimental realisation is described in detail.

2.1 Segment 1 - Laser Sources

Two different light sources are used: the first laser is a self constructed, distributed feedback laser (DFB) from the 5. Physical Institute (University of Stuttgart),whereas the second source is a commercial diode laser from Toptica (DLPro series)[16].
The DFB laser does not have an inbuilt optical isolator. Therefore, an additional optical isolator has to be integrated to protect the laser from feedback due to back reflections.
The wavelength of both lasers is 780 nm. Technically, it is not necessary to use two lasers since the laser beam is split and interfer with it-self, but in this way it is possible to see if there are differences caused by the coherence and the collimation properties of the laser light.
The basic task is to align the beams of the two lasers in a single point. For this reason a non-polarizing beam splitter cube (50/50 cube, BS), with a transmission and reflection of 50%, is used.
In order to use both lasers without changing anything on the beam path setup, the lasers have to be aligned in intensity and beam width. This alignment is necessary to achieve the same amount of light coupled into the fibre. Moreover, by comparing the data sheets [16] of the two lasers, the beam width of the DFB laser has to be reduced by approximately two-thirds of its width. This is also necessary to send the beam trough the beam modulation devices in section 2.
To this end, a telescope with a magnification (M) of $M = \frac{30\,\mathrm{mm}}{100\,\mathrm{mm}}$ is used[17]. For coupling purposes the beam width is measured with two different methods. The first method employs a blade which is moved through the beam, the other method uses a Shack-Hartmann-Sensor to determine the beam width.

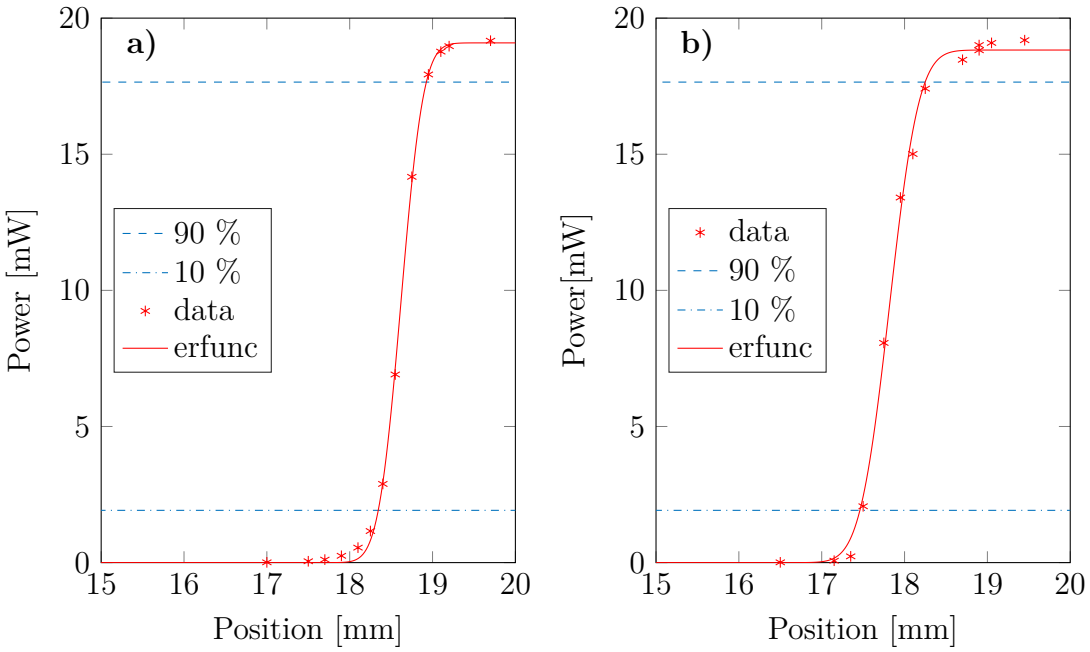

Figure 2: Measurement of the laser intensity as a function of the position of the blade for a DFB laser (a) and a DLPro laser (b).

With the blade method it is possible to determine the horizontal beam width and its shape (see Fig.2)As the fitted line in the figure depicts. the beam shape can be accurately modelled with an Gaussian error function (finite integral over a Gaussian distribution). The beam width is 0.79 mm for the DLPro laser and 0.81 mm for the DFB laser. The horizontal waist positions differ approximately by 1.1 mm. Unfortunately, with this method only the horizontal position of the beam may be determined. To align the two lasers properly on a common point a two-dimensional alignment of the beam paths is necessary. Therefore, a Shack-Hartmann-Sensor is employed.To adjust the beam widths, and to collimate the beams in order for them to pass through the exact same horizontal and vertical position.

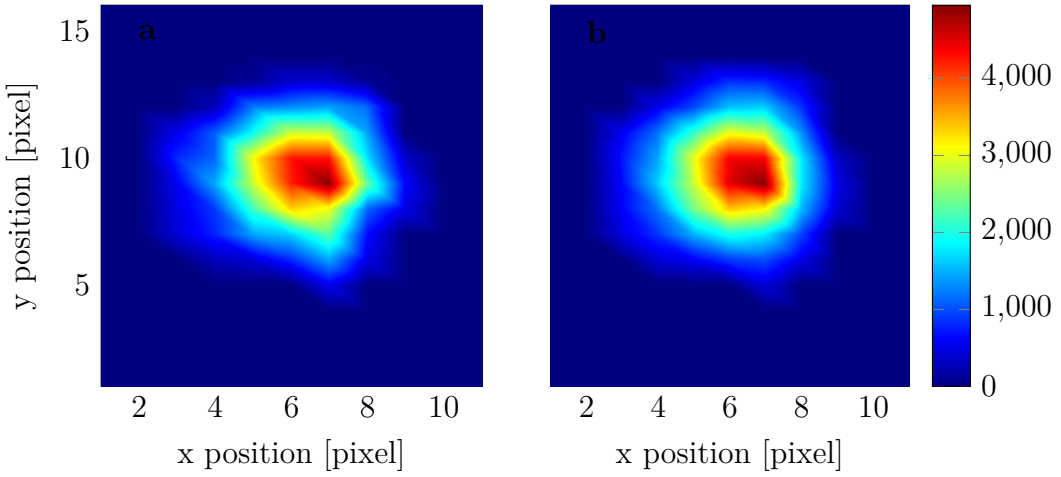

Figure 3: Measurement of the beam position with a Shack-Hartman-Sensor. For a DFB laser (a) and a DLPro laser (b). The laser intensity (colour coded) is plotted as a function of the horizontal and vertical position on the sensor measured in pixels.

The intensity of the lasers was reduced by filters to protect the sensor. The Shack-Hartmann-Sensor is able to calculate the beam width of an incoming beam automatically. The automatically determined beam widths are 0.8 nm for the DFB laser and 0.8 nm for the DLPro laser. With a pixel size of 0.2 nm this leads approximately to the same results measured with the blade method.

2.2 Segment 2 - Interferometer

In this segment of the experimental setup the aligned laser beam during the first module is split and modulated in phase and frequency. Subsequently, both laser beams are recombined and interfere with each other. In the following, the devices, which are used for this purpose are presented and explained in more detail.

2.2.1 Polarising beam splitter

With the help of a polarising beam splitter (PBS) the beam is divided into two polarised beams: one beam with horizontal polarisation and the other with vertical polarisation. The advantage of this beam splitter is, that with the help of a lambda half plate the intensity distribution of both beams may be varied. This is necessary to maintain a perfect balance of the intensities after the fibre coupling.

2.2.2 Electro-optic modulator

The electro-optic modulator (EOM) uses the Pockels effect which is an electro-optic effect to modulate the phase of a light wave, with the help of a birefringent crystal and capacitor plates. A change of the electric field causes the refractive index to change. This modification of the refractive index of a non-linear crystal, which is used for the Pockels cell, changes proportional to the strength of the field [18]. The material, which is used in this case, is a MgO:LiNbO3 crystal and has different refractive indices along the different crystal axes. This implies that the effect of the crystal depends on the orientation of the crystal axes in relation to the electric field. Further more, the polarisation of the wave propagating through the crystal is another important factor which has to be considered. It can be shown theoretically [20] that the index of refraction as a function of the electric field may be expressed as:

$$n(E) = n_0 - \frac{1}{2} \cdot r_{eff} \cdot n_e^3 \cdot E, \tag{2.1}$$

where n_0 describes the refractive index in the absence of an electric field. The coefficient r_{eff} is the Pockles coefficient, which affects the incoming laser beam, n_e is the refractive index in the presence of an electric field and the electric field of the parallel-plate capacitor itself is described by E.[19] A constant phase shift, is by n_0, however in our case the the voltage dependent phase shift is of more relevance. Therefore, only considering the relative phase shift, the equation can be re-written as

$$\Delta n(E) = \frac{1}{2} \cdot r_{eff} \cdot n_e^3 \cdot E, \tag{2.2}$$

which describes the change of the index of refraction merely due to the electric field. To obtain the phase shift resulting from a change of the refraction it is necessary to know the magnitude of the phase shift

$$\Phi = \frac{2 \cdot \pi}{\lambda_0} \cdot n \cdot L \tag{2.3}$$

that the light beam picks up, by propagating through a non-linear medium.[20] λ_0 describes the wavelength outside the medium, n the refractive index of the medium and L describes the length the beam has to travel through in the medium. Assuming that the capacitor is a perfect parallel-plate capacitor which produces an electric field,

$$E = \frac{V}{d} \tag{2.4}$$

with dependency on the applied voltage V and the distance d between the plates. The phase shift may be described as

$$\Phi = \frac{L \cdot \pi}{\lambda_0} \cdot n_e^3 \cdot r_{eff} \frac{V}{d}. \tag{2.5}$$

The refractive index also depends on the wavelength of the laser beam. The dependency of the index of refraction on the wavelength is given on the specification sheet of the

crystal[21]. Hence for a laser wavelength of 780 nm, the refractive index of the crystal with an applied electric field was calculated to be

$$n_e(\lambda) = \sqrt{4.5469 + 0.094779/(\lambda^2 - 0.04439) - 0.026721 \cdot \lambda^2} \tag{2.6}$$

$$\Rightarrow n_e(780) = 2.16765. \tag{2.7}$$

Now using the properties of the crystal and the properties of the optical setup the phase shift can be calculated. The phase shift in dependency of the voltage could be calculated. Therefore, the resulting phase shift may be expressed purely as a function of the applied voltage (as illustrated in Fig.4).

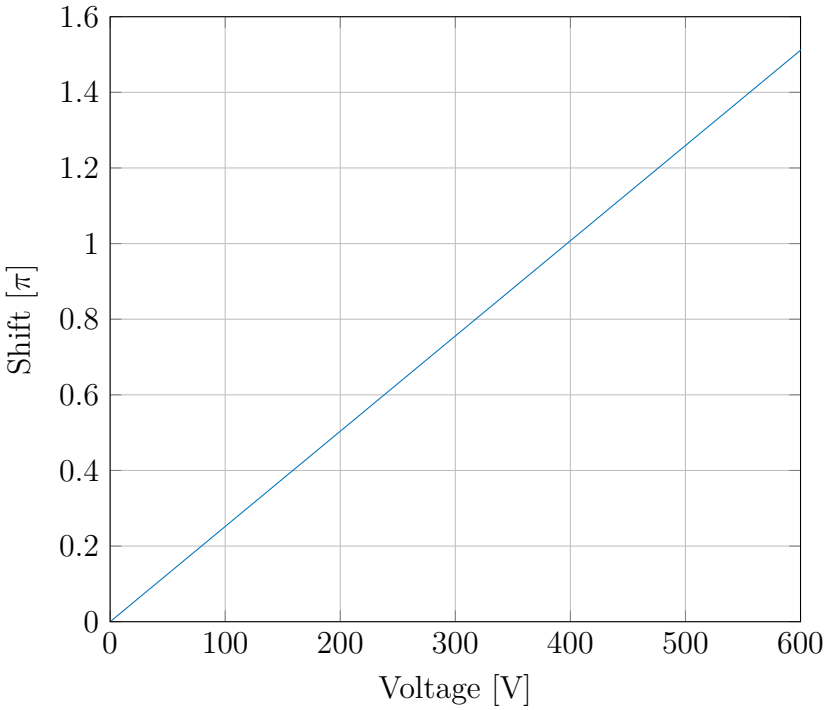

Figure 4: In this diagram the shift in units of π is plotted as a function of the applied voltage. In this case the wavelength is 780 nm and the electro optic coefficient r_{eff} is 30.7 pm/V[21]. The graph shows, that approximately 400 V are necessary to reach a shift of π on the signal beam.

To reach a phase shift of π a high voltage power supply of up to 500 V from Applied kilovolts was used. Nonetheless, applying such a high voltage to a standard metal case can produce sparks between the capacitor plates. To avoid the sparkling between the two metal parts the case was redesigned and 3D-printed out of polyactide plastic. The final output voltage of the capacitor may be regulated by means of a second control voltage in a much lower range of $1 - 10$ V. The output voltage then adopts a linear dependence on this control voltage. One important point was that the electric field of the capacitor should be switchable. Therefore a high voltage switch was used. Because this switch was used for the first time some basic characterisations, which could effect the setup.

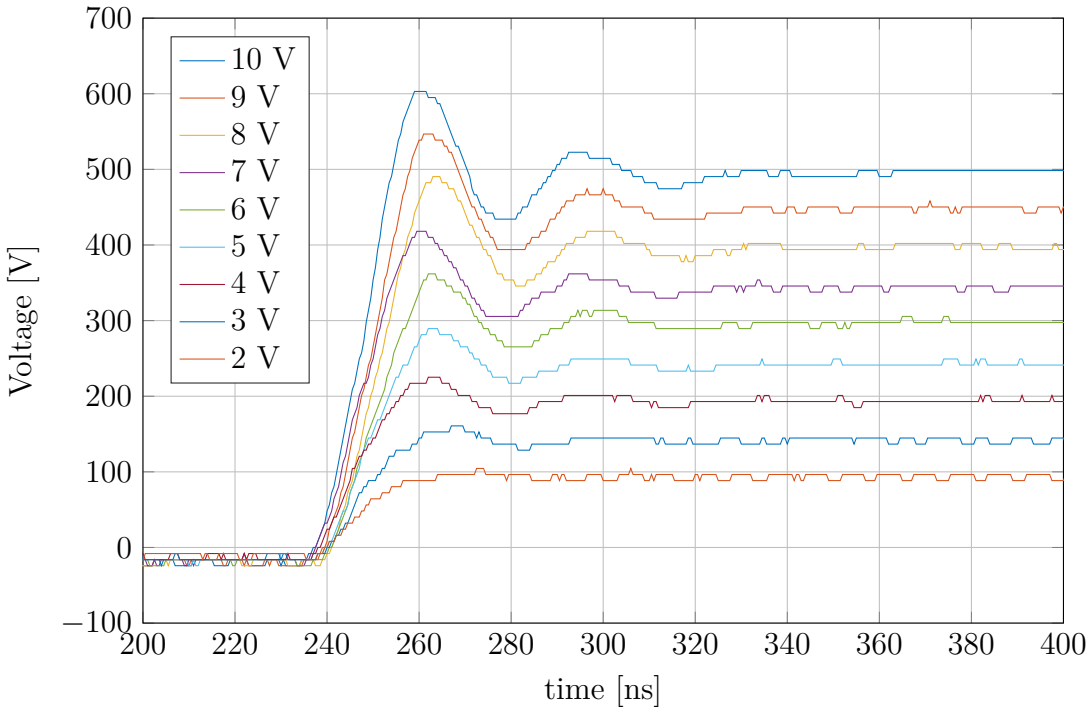

Figure 5: Plot of the capacitor voltages as a function of time after the switch is flicked. Various line colours (see legend) indicate different levels of control voltage. An average rise time of $24.5 \pm 2\,\mathrm{ns}$ is observed for different control voltage levels likewise a voltage overshoot of ca. 20% ±4 on average occurs for all control voltages. An negative offset is noticeable, which decreases linear with a rising level of the control voltage.

The above mentioned overshoot of the output signal produces noise on the interfered measurement signal, which has to be considered at later measurements. Furthermore, the ratio between the control and amplified voltage was calculated to be $Volt_{out}(x) = 52.3 \cdot x$ with x as a variable for the applied control voltage. In addition the dead time of the switch and the signal delay time of the switch are measured. The measurement of the dead time yield to a highest possible switching frequency of 500 kHz. A higher switching frequency will cause voltage loss at the output signal. The delay time of the switch was 496 ns, which is in accord with the data from the specification sheet of the switch [22].

2.2.3 Acousto-optic modulator

To gain a frequency difference between the split beams an acousto-optic modulator (AOM) was used. The AOM uses the acousto-optical effect to diffract the incoming laser light into different orders through the following mechanism:
Stimulation of a piezo-electric transducer with an oscillating electrical signal results in acoustic waves propagating through a dense, highly refractive material, such as a special type of glass or crystal. The standing wave created in the material, leads to a density chance, which, in turn, causes a change of the refractive index of the material. Due to

the fact that the simulating frequency is much lower than the frequency of the light, the standing wave in the transmitting material acts like a diffraction grating to the incoming laser beam.

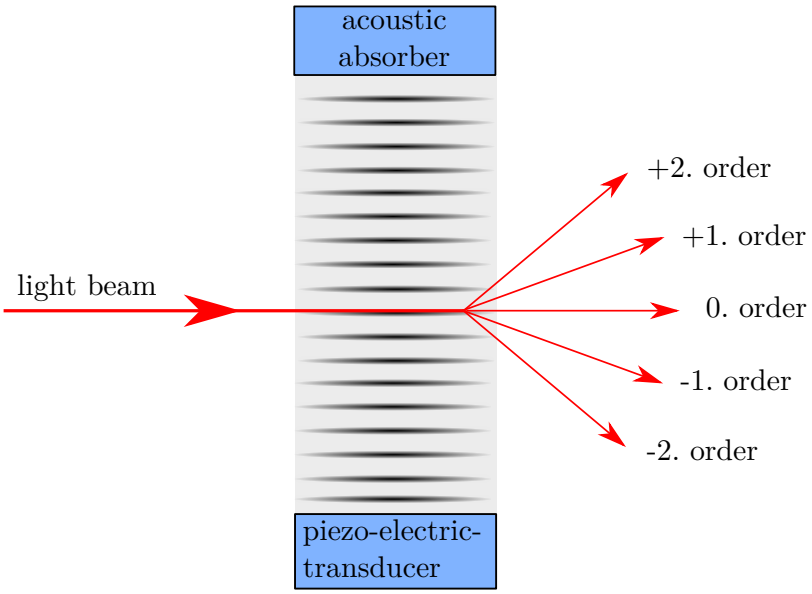

Figure 6: Principle of an AOM (simplified): incoming laser light propagates through the crystal of the AOM. Due to the acoustic modulation of the crystal, the laser beam is diffracted into different orders. These orders appears in angles of the Bragg regime.

A standing wave in a material does not shift the frequency of the incoming beam. Therefore the beam has to be scattered on moving plans. The consequent for the incoming beam is a Doppler-shift by the amount of the diffraction order times the driver frequency. In order to gain a frequency shift of 80 MHz driver frequency of 80 MHz is applied to the AOM and the first positive order is used. The negative first order may also be used instead. The benignity of the driver frequency is checked with a spectrum analyser to be capable to determine the frequency and resultant the period time.

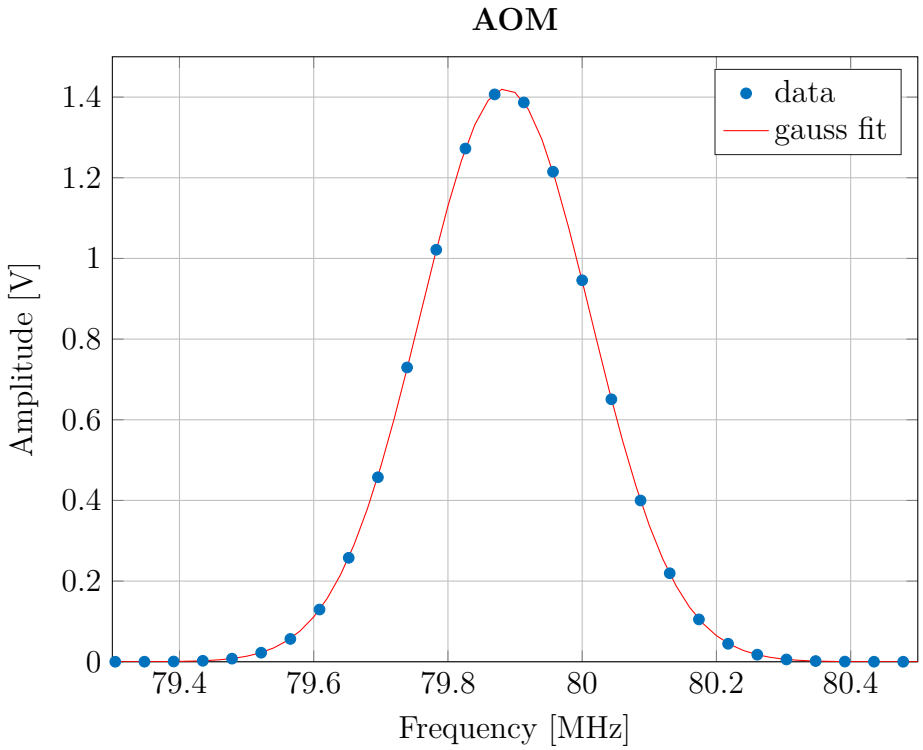

Figure 7: Measured frequency spectrum of the AOM driver signal and Gaussian fit with a peak at $79.89 \pm 0.01\,\mathrm{MHz}$. The beat width, defined by twice the width of the Gaussian function, is $356\,\mathrm{kHz}$.

2.2.4 Power balancing

Interference of light is a well-researched and discussed topic [23]. For this experiment it is important to descry how to reach the most effective interference between the two laser beams. One conclusion from basic interferometry is that to create effective interference it is important for the beams to be well balanced in intensity.

The power of the lasers are measured at different positions (see Table 1) and as best as feasible matched with each other by compromising between splitting the beams effectively and generating sufficient (but not excessive) power after the coupling.

Position	DLPro	DFB
Pos. 1	7.04 mW	5.96 mW
Pos. 2	7.12 mW	6.01 mW
Pos. 3	5.03 mW	4.37 mW
Pos. 4	1.95 mW	2.03 mW

Table 1: Intensity of the beam paths at different positions. Position 1: path through the AOM, just after the AOM. Position 2: path through the EOM, just after the EOM. Position 3: before the fibre coupler. Position 4: after the fibre coupler. Crucial position for the power measurement is position 4, since excessive beam intensity reaching the photon counter could destroy it.

When coupling the light into the single-mode fibre, approximately half the power is lost (remaining power after coupling: 38-46%). Despite the power loss this coupling mechanism has multiple benefits: firstly, by coupling the beams of both arms of the interferometer into a singe fibre, interference is drastically improved; secondly, the use of a single-mode fibre prevents the occurrence of other modes in the beam. To balance the power between the two arms a PBS cube is used to control the intensity for the transmission and reflection of the beam with a lambda-half plate (see above). Furthermore, interference can only take place if the overlapping beams have the same polarisation. Because of this circumstance, another lambda-half plate has to be used in one of the interferometer arms to rotate the polarisation by 90 degrees.

2.3 Segment 3 - Measurement

This section describes the different measurement methods, which are used to measure the phase shift produced by the EOM. After the coupling of the laser beam in module 2, the beam is out-coupled and split with a BS. One the resulting beams is measured with a classical photodiode, while the other beam is measured with a single photon counter module.

2.3.1 Photodiode

For the classic measurement of the modulated sinus signal a self-built photodiode is used. In this device a photosensor from Hamamatsu G4176-03 is obstructed. To amplify the signal from the photodiode radio frequency amplifiers (Bias-Tee MiniCircuits ZX85-12G+, MiniCircuits ZX60-8008E+) are used. This photodiode outputs an alternating current (AC) signal. Which creates the advantage that only the beat frequency is detected and not the offset of the signal.

2.3.2 Single photon counter module

In the other type of measurement, the signal is detected with a single photon counter module (SPCM) (Excelitas). This SPCM uses a unique silicon avalanche photodiode (SLiK), which leads to a dead time of only 24 ns. Also a peak photon detection efficiency greater than 70% at 700 nm over a 180 μm diameter can be achieved. The maximum counting rate of this module is 5 million counts per second. This value shouldn't be exceeded or it can cause damage to the SPCM. If a photon gets detected, the SPCM outputs a transistor-transistor logic (TTL) pulse with an amplitude of 1.5 V. [1]

2.3.3 FPGA based pulse generator

To generate controlling pulses for the EOM and the measurement devices, a field-programmable gate array (FPGA) based pulse generator with a nano-second precision is used. This pulse generator was developed by Dr. Helmut Fedder and the 5th physical institute of the university of Stuttgart. The testing and characterisation of this device were done by Felix Engel in his Bachelor thesis. [2] With this pulse generator it is possible to generate nano second pulses with an accuracy of 0.4 ns. This accuracy of the pulses was necessary for the trigger pulses of the time-tagger.

2.3.4 FPGA time-tagger

For the measurement of the photon pulses a FPGA based time-tagger[3] is used. This FPGA based Time-Tagger can detect up to eight independent channels with a time resolution of 60 ps. If a pulse reaches the FPGA chip, which is higher than a specified trigger level, a time tag is saved at the buffer memory of the time-tagger. Subsequently, the time tag is sent via USB2 to a computer. It is temporary stored in the random access memory of the computer. However, the bit rate of the USB2 and the FPGA chip are limited by a total counting rate of 5 million counts per second for all channels.
For later discussions about the data analysing it is essential to understand the concept of the save files. The measurement starts with a trigger pulse which is applied on an input channel of the time-tagger. It counts the incoming photon pulses for a specified number of bins (line width). The detected counts are saved as a time tag in an array, where the column number is the number of bins for a fixed time interval. The measurement time is defined by the column length of the array times the bin size. If there is a trigger pulse for a new measurement during the measurement time the pulse will be ignored, otherwise the trigger pulse will start a new shot row. The new shot array would be saved in the next following row of a matrix. Consequently the final save file is a matrix with (number of shot) x (number of bins).

[1] Spec.:delaytime= 40 ns; dark counts < 250 counts/s (confirmed). All of this information are taken from the specification sheet of the SPCM.[24]

[2] Entwicklung eines FPGA basierten Pulsgenerators mit Nanosekunden-Auflösung fur schnelle Rydberg-Experimente by Felix Engel

[3] This time-tagger prototype was developed from the 3rd Physical Institute as well as the controlling software.

2.3.5 Alignments

Classic Signal

As explained above a single beam is split into two separate beams with almost identical intensity. The beam for the classical measurement is focused with a lens and then detected with an AC photodiode. The signal, which reaches the photodiode has an intensity of 0.7 mW. The photodiode produces a sinusoidal output signal with an amplitude of 50 mW. This amplitude can be measured with an oscilloscope. As a result of the low amplitude the time-tagger has difficulties to find an appropriated trigger level. Moreover, the time-tagger is only able to detect positive input voltages. Therefore the sinusoidal signal is offset with a Bias-Tee. Since the time-tagger can detect signals with a sharper slope more precisely than a low amplitude the signal was amplified by a factor of two with a radio frequency amplifier and then send to an RF switch. This was necessary because the time-tagger can only detect continuous signals up to 5 million counts per second. A frequency of 80 MHz would produce 80 million counts per second. This would lead to a buffer overflow. Therefore, the signal is switched to reduce the number of counts which reach the time-tagger to an average amount of 3 million counts per second.

Single-photon Signal

For the SPCM measurement to be successful, some modifications have to be made to the setup. First, the beam has to be coupled into a single-mode fibre to send the light to the SPCM. Because of the limitation of the SPCM, the intensity of the beam has to be attenuated by optical filters. The attenuation of the filters can be calculated by knowing the intensity of the incoming laser beam and some basic light properties. Finally there should a counting rate of 1 million counts per unit time. Therefore the attenuation O is calculated as:

$$P_{\text{1Mio}} = n\frac{h \cdot c}{\lambda} = 2.5 \cdot 10^{-13}\text{W} \tag{2.8}$$

$$P_{\text{laser}} = 0.8 \cdot 10^{-3}\text{W} \tag{2.9}$$

$$\rightarrow O = 10^{10} \tag{2.10}$$

To be safe, first more filters than necessary are used and then experimentally reduced until the target counting rate is reached.
For the SPCM alignement the dark counts have to be determined. Therfore the laser emissions were turned off and only with fibre attached the SPCM was turned on. To prevent light from the room to couple into the fibre and to reduce the dark count well below 1500 counts/s a 780 nm bandpass filter is mounted in front of the lens of the fibre coupler. With this additional filter an average dark count rate of 254 counts/s could be reached.

3 Classical Measurement

This section describes the different measurements carried out during the bachelor thesis and presents the obtained results. Starting with the classical measurement of the phase shift with an oscilloscope and followed by the classical measurement with the time-tagger.

3.1 Classical Signal

For the discussion of the different measurement methods, it is important to understand the different theories of light. The following description of the classical light theory is based on the chapter "Classical optics" in Mark Foxs book "Quantum Optics - A Introduction" [25]. There more information and derivations of the equations can be found.

The description of classical light used in this thesis is based on the Maxwell's equations. The electromagnetic waves are described by the electric field $\boldsymbol{E}$, the magnetic field $\mathbf{B}$, the electric displacement $\boldsymbol{D}$, and the magnetic quantity $\boldsymbol{H}$. Then, the four laws of electromagnetism in their differential form may be expressed as:

$$\boldsymbol{\nabla} \cdot \boldsymbol{D} = \varrho, \tag{3.1}$$

$$\boldsymbol{\nabla} \cdot \boldsymbol{B} = 0, \tag{3.2}$$

$$\boldsymbol{\nabla} \times \boldsymbol{E} = -\frac{\partial \boldsymbol{B}}{\partial t}, \tag{3.3}$$

$$\boldsymbol{\nabla} \times \boldsymbol{H} = \boldsymbol{j} + \frac{\partial \boldsymbol{D}}{\partial t}. \tag{3.4}$$

Where the free charge density is ϱ and the free current density is $\boldsymbol{j}$. The first equation is called Gauss'law of electrostatics, the second Gauss law of magnetostatics, and the third equation is a combination of the Lenz's and Faraday's laws and thus Gauss law of electromagnetic introduction. The fourth equation is Ampere's circuit law with Maxwell addition. For further informations and the derivation of the Maxwell equations there is a detailed chapter about Maxwell equations in Hecht 2002.
With the use of a vector identity and the assumption that there are no free charges ($\varrho = 0$) or currents ($\boldsymbol{j} = 0$) equation 3.4 may be written as

$$\boldsymbol{\nabla}^2 \boldsymbol{E} = \nu_0 \epsilon_0 \epsilon_r \frac{\partial^2 \boldsymbol{E}}{\partial t^2}, \tag{3.5}$$

where the electric displacement was substituted with $\boldsymbol{D} = \epsilon_0 \epsilon_r \boldsymbol{E}$. Therein, ϵ_0 describe the electric permittivity of free space which is given as a constant of $8.854 \cdot 10^{-12}$ Fm^{-1} in the international system of units (SI). The relative permittivity of an arbitrary medium is given by ϵ_r.
With equation (3.5) the speed c of the propagating electromagnetic wave in free space

($\epsilon_r = 1$) is given by

$$c = \frac{1}{\sqrt{\nu_0 \epsilon_0}} = 2.9998 \cdot 10^8 \mathrm{Fm}^{-1}, \tag{3.6}$$

For a dielectric medium which has a $\epsilon_r \neq 1$, the speed of the propagating wave is given by:

$$\upsilon = \frac{1}{\sqrt{\epsilon_r}} \cdot c \equiv \frac{c}{n}, \tag{3.7}$$

The refractive index n of a dielectric medium relates to the optical properties of the medium through:

$$n = \sqrt{\epsilon_r}. \tag{3.8}$$

The change of the speed of propagation of the wave through the medium causes phase shifts.
The magnetic and electric fields are orthogonal to each other. So considering a wave which propagates in the z direction and with a frequency of ω, the solution of Maxwell's equation is of the form:

$$E_x(z,t) = E_{x0} cos(kz - wt + \phi), \tag{3.9}$$
$$B_y(z,t) = B_{y0} cos(kz - wt + \phi). \tag{3.10}$$

Hence, the amplitude of the wave is given by E_{x0}, ϕ describes the optical phase (which can be used to identify the phase difference) and k as the wave vector given by:

$$k = \frac{2\pi}{\lambda_m} = \frac{\omega}{\upsilon}, \tag{3.11}$$

with λ_m being the wavelength inside the medium. Alternatively, in complex notation, one may also write the solution in the following form and then take the real part when converting to real, measurable quantities:

$$E_x(z,t) = E_{x0} e^{i(kz - wt + \phi)}, \tag{3.12}$$
$$B_y(z,t) = B_{y0} e^{i(kz - wt + \phi)}. \tag{3.13}$$

By splitting an incoming beam with a PBS, the wave is separated into two orthogonally polarized beams. After they are split, the beams are linearly polarized. This means that the electric field vector only points along one direction. If both beams should interfere with each other, the electric field vectors of both beams have to point into the same direction.
There are many different ways to achieve interference. One of the most common interferometers is the Michelson interferometer. This interferometer uses the variability of the beam path length to generate a beam length difference and therewith interference. During the experiment of this bachelor thesis another method was used, as explained in section setup. In this setup the interference and the output voltage of the photodiode can

be written as a function of two lasers with two different frequencies ω_1, ω_2 as a function of the time t.

$$V_{PD} \sim (Acos(\omega_1 t) + Bcos(\omega_2 t))^2 = \frac{1}{2}(A^2 + B^2) + \frac{1}{2}(Acos(2\omega_1 t) + Bcos(2\omega_2 t)) \quad (3.14)$$

$$+ ABcos((\omega_1 + \omega_2)t) + ABcos((\omega_1 - \omega_2)t) \quad (3.15)$$

$$\rightarrow ABcos(\omega_b t), \quad (3.16)$$

Hence, the $ABcos((\omega_1 - \omega_2)t)$ term describes the beat frequency of the resulting wave. Since in this setup an AC photodiode is used, the resulting wave has a frequency $\omega_b = |\omega_1 - \omega_2|$. The other DC terms are filtered out by the AC photodiode.

3.1.1 Oscilloscope Phase Shift Measurement

The measurement of the classic signal is detected with a photodiode, which produces a sinus signal with a frequency of approximately 80 MHz. This signal is measured with an oscilloscope. The pulses and signals are visualised in the following figure (see Fig. 8).

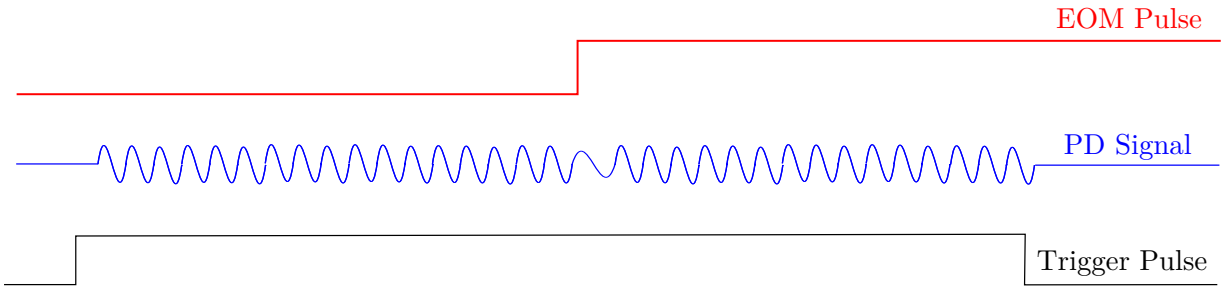

Figure 8: This pulse scheme shows the signals which are used for the measurement of the classical phase shift. The EOM pulse is the main pulse for this measurement. All other pulses are related to the 5 kHz square EOM pulse. The trigger pulse of the oscilloscope has a width of 5000 ns **and is centred on the rising edge of the EOM pulse.**

Coherence

First, the coherence stability of the laser for the measurement time has to be confirmed. Therefore, a time interval of 5000 ns is measured with a resolution of 0.5 ns. This is the longest time interval, which could be measured with the oscilloscope and avoid the loss of resolution. A lower resolution leads to inaccuracy during the fit. To determine the phase stability two sinus functions are fitted and compared: one sinus is fitted to the first 1000 ns of the measurements; the other sinus is fitted to the last 1000 ns.

The fit function is of the form:

$$\text{fit} = A \cdot sin(2\pi bx + 2\pi bc) - d, \tag{3.17}$$

where A describes the amplitude, b the frequency, c the phase and d is the offset of the signal. For a measurement which verifies the coherence of the laser beam all parameters [1] should stay constant. However, the crucial parameters are the frequency and the phase of the signal. The frequency of the fits should correlate with the driver frequency of the AOM, as explained in the introduction in the section "Classical Signal". The first fit function leads to a frequency of 79.896 ± 0.001 MHz. The second fit has a frequency of 79.896 ± 0.001 MHz. Within the inaccuracy the frequencies of the two fits are the same. Likewise the comparison with the driver frequency verifies the results of the fit.

[1] fit 1 + fit 2: amplitude = 206 mV, offset = −6 mV

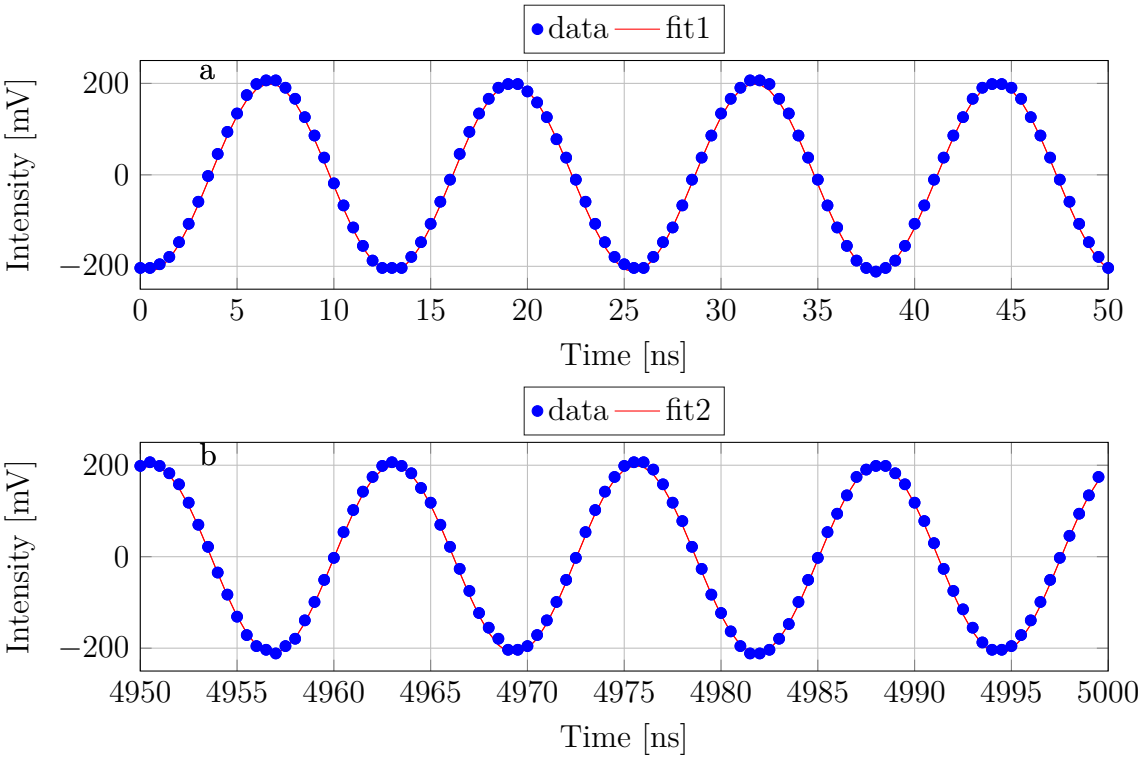

Figure 9: The measured intensity output of the photodiode as a function of time. In diagram (a) the first 50 ns of the measurement are visible. A sinus function is fitted to the data points. In graph (b) the last 50 ns are visible. There another sinus function is fitted to the last data points excluding the first ones.

Subsequently, the parameter for the phase is compared. The fit at the beginning of the measurement determines a phase of -3.574 with confidence bounds of (-3.579, -3.569). Whereas the fit function at the end of the measurement time has a phase of -3.585 with a high and low confidence bound of (-3.598, -3.573). The difference between the phase parameters is 0.011 which is only 0.09 % of the total period if we consider a period of 12.5 ns and within the confidence bounds. Therefore the coherence over a time of 500 ns can be confirmed. The measurement of the DLPro laser is summarised in the following table (Tabel 2).This confirms the phase and frequency stability for both laser, to measure over a time interval of 500 ns.

Parameters	values	confidence bounds
b_1	0.0798924	(0.0799, 0.0798)
b_2	0.0798918	(0.0799, 0.0798)
c_1	-5.482	(-5.487, -5.479)
c_2	-5.479	(-5.473, -5.482)

Table 2: In this table the parameters of the two sinus fits for the DLPro laser are listed. The indices describe, whether they belong to the fit at the beginning (index = 1) or to the fit at the end (index = 2) of the measurement. The frequency of both fits is within the error range of the fit function and correlate with the driver frequency. The difference between the phase parameters is 0.003, which is less than the phase difference of the DFB laser.

Phase shift

The analysis of the classical phase shift measurement with an oscilloscope is calculated similar as the phase stability measurement before. The pulse scheme illustrated in Fig. 8 was used to trigger the measurement devices.

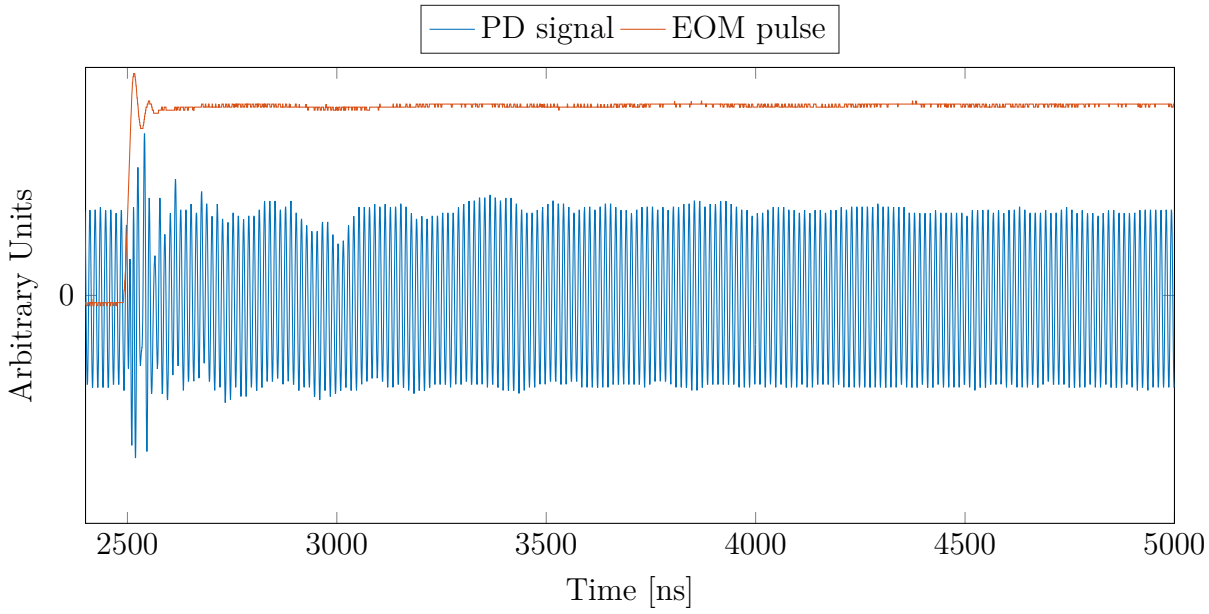

Figure 10: In this diagram the photodiode signal and the pulse signal of the EOM are plotted over the time. Noise appears on the EOM signal. 1500 ns **after the EOM pulse the noise on the signal has normalized. Moreover, there is no noise on photodiode signal before the EOM pulse reach the crystal.**

Because before the shift there is no noise on the signal, probably the EOM causes the noise. A reason may be a small expansion of the crystal, which causes a small displacement of

the beam. Consequently, this will change the intensity of the interference. The pulse for the EOM is timed in the middle of the measurement. To reach a continuous signal before and after the shift the signal is measured 1500 ns before and after the shift. Despite the fit can be longer the same time interval is used to receive the same conditions for both fit functions. In the following, the analysis method is explained with diagrams.

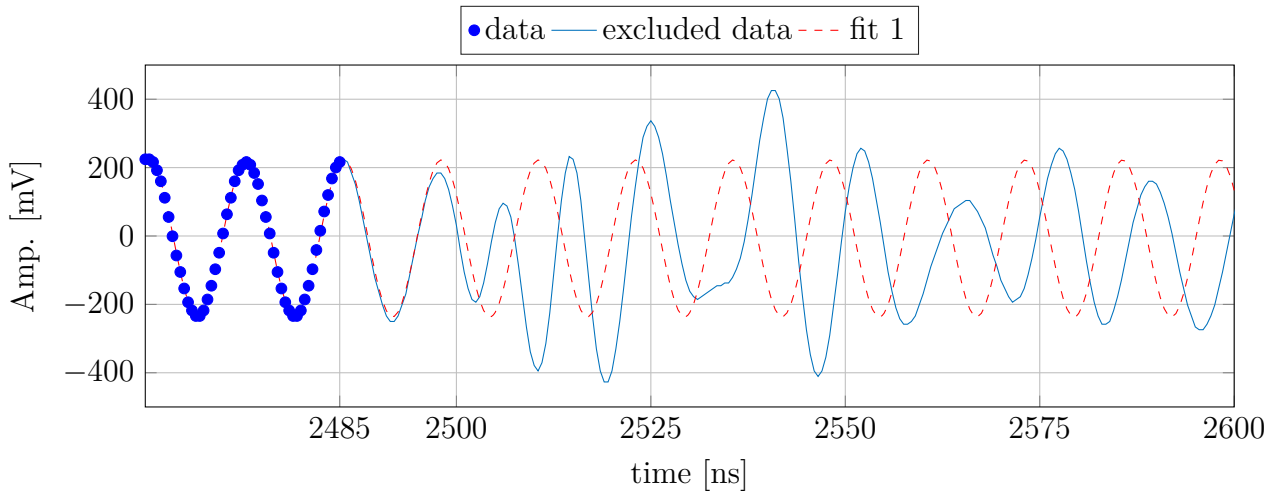

Figure 11: This diagram shows the amplitude of the photodiode signal over the time. For demonstration purposes function is fitted up to 2485 ns. While the data points after 2485 ns are excluded, to produce a signal to compare with and without phase shift. The high voltage pulse, which causes the phase shift in the EOM, starts at 2495 ns. During the next 24.5 ns which is the rising time of the switch the phase is shifted to its final phase. Another shift is noticable between 2425 ns and 2550 ns, which is probably caused by the drop of the overshooting of the HV switch pulse. The fit function describes the development of the signal without phase shift. The signal is shifted in the forward direction of the propagating wave. This means the distance between two following maxima increases, during the shift happen. By rotating the crystal by 180 degree distance between the maxima will decrease, hence the shift would be in the other direction.

This measurement is done for power supply control voltages in a range of 1 Volt to 10 Volts and the two fitting areas. Subsequently, the two fits are compared with each other. Therefore the difference between the prior fit1 and the fit2 after the EOM pulse are determined.

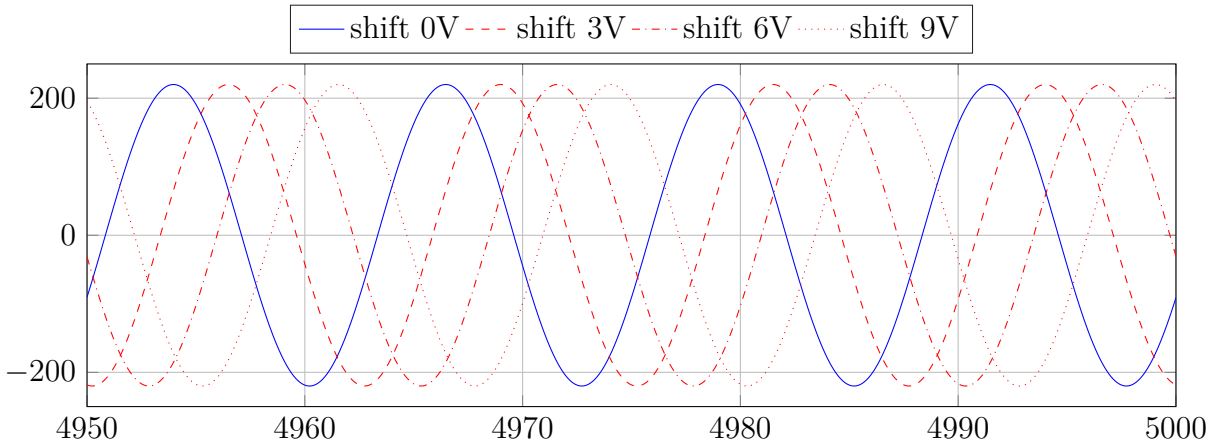

Figure 12: This diagram shows the the last 50 ns of the measurement. The blue zero Volt measurement is the signal fit without electric field attached. Hence there is no phase shift. This is the reference signal. All other measurements in this plot are regarding to this. Thereby, the red graphs are the signal fit after the phase shift. The voltage in the legend is the control voltage of the high power supply. Moreover, the diagram shows that the phase shift is increasing with rising control voltage as expected.

The previous figures are measured with the DFB laser. Also the DLPro laser is measured with the same method. The measurements are made for different voltages to be able to fit a linear function through it and compare the experimentally measured data with the theoretically calculated values. The classical phase shift measured with the oscilloscope fits nearly to the theoretically calculated values (see Fig. 13). The slope is lower than the theoretical one. This different may be explained by the distributions in the electric field of the EOM and an oscillation around the the output voltage of the high power supply. Because of the fine differences in the diagram the raising functions are calculated. This will give a better possibility to compare the functions with each other.

$$\Phi_{\mathrm{DFB}}(V) = 0.1345 \pm 0.001 \cdot V \tag{3.18}$$

$$\Phi_{\mathrm{DLPro}}(V) = 0.1348 \pm 0.001 \cdot V \tag{3.19}$$

$$\Phi_{\mathrm{theory}}(V) = 0.1359 \cdot V \tag{3.20}$$

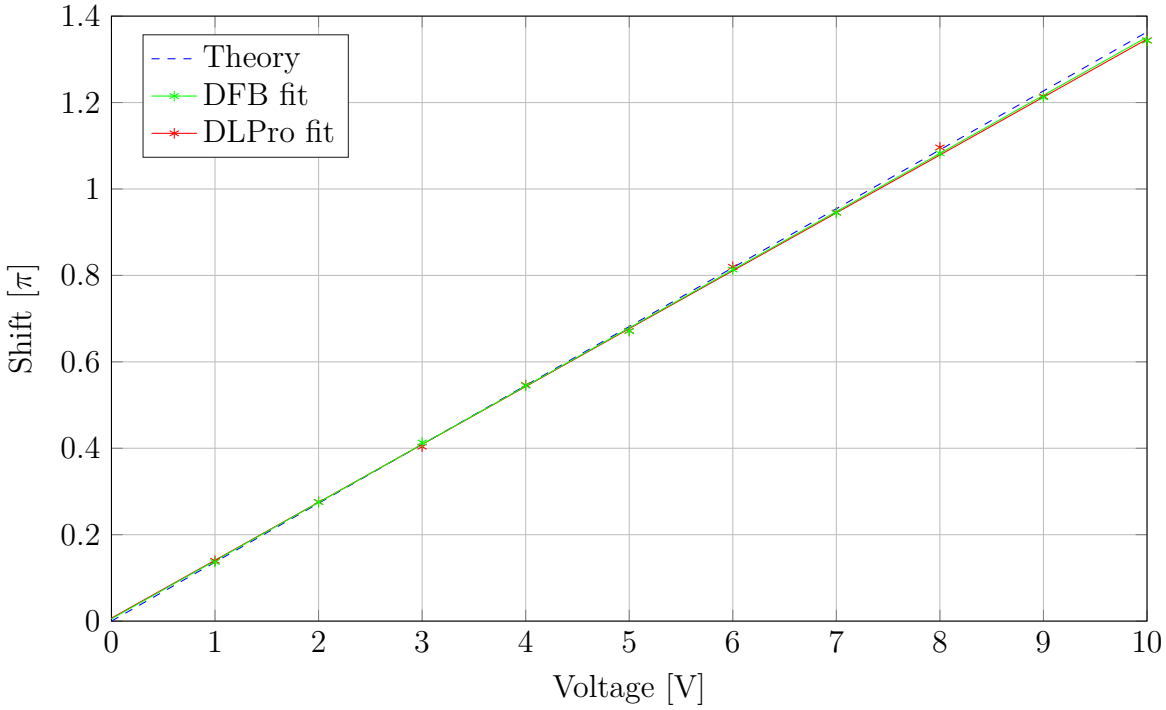

Figure 13: In this diagram the phase shift in units of π is plotted over the control voltage. Thereby the theoretically calculation of the phase shift is also plotted. Both laser have quite similar results for the phase shifts as a function of the control voltage.

3.1.2 Time-Tagger Phase Shift Measurement

Due to the advanced setup with a time-tagger the classical phase shift can be measured with another methode. Therefore the classical signal of a photodiode was detected with the time-tagger. As mentioned the frequency of the signal is to high for the buffer memory of the time-tagger and run into a buffer overflow as a result of to many tags per second. This leads to messy measurement data with arbitrary filled measurement arrays. The solution is to pulse the signal with an RF-switch. The signal which now reach the time-tagger has recovering times between the signal pulses. This recovering times keep the total number of counts under 1 million/s.

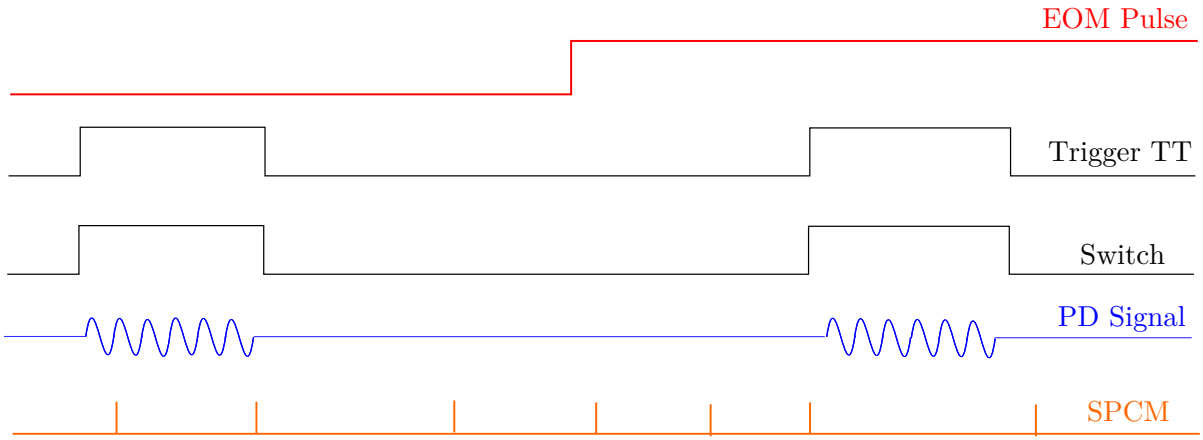

Figure 14: This graph shows the pulse scheme of the different devices. The main signal is the pulse signal of the EOM every other pulse is related to this signal. The trigger signal (black) for the time-tagger is used to start a new measurement row and to switch the photodiode signal with the RF-switch. The EOM pulse signal is still a pulse with a frequency of 5 kHz and a duty cycle of 50 % as used for the oscilloscope measurement. The switch signal instead has two pulses with the same frequency as the EOM signal to be able to measure before and after the shift, with a pulse width of 1000 ns and a time difference of 3000 ns between the measuring pulses. The total measurement time of 5000 ns is in the verified coherence time of the laser.

This measurement outputs a 5000 times 2000 matrix because the bin size of the time-tagger was set to 0.5 ns. The odd rows are the measurement prior the phase shift. Consequently, the following even row numbers are the measurement pulses after the phase shift. Primarily, the row save file matrix is separated into an even and an odd row number matrix. Therefore, one matrix will contain the time tags prior the shift the other matrix will contain the time tags after the shift. It is important to start with a low trigger signal for this time-tagger. If not the first row will be the measurement after the shift and has to be skipped for the sorting to start the sorting with the correct matrix. For the analysis of the time-tagger measurements two different methods are use: one uses the differences of the time tags between the prior and after shift matrix, the other method maps the

time tags on a unit circle to use the angle difference to calculate the phase shift. For both methods the frequency has to be known very precisely.

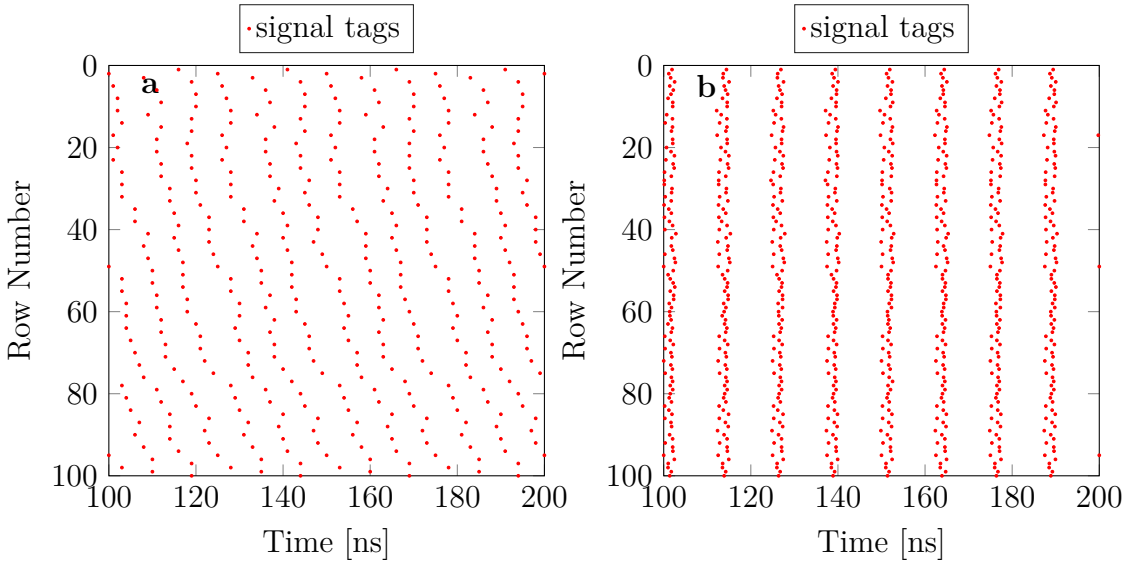

Figure 15: In this figure the time tags of the matrix prior the phase shift is plotted. The y axis describes the number of rows, the x axis is the number of bins. The number of bins can be re-written as time, as shown in this figure. In figure (a) a part of the row prior matrix is visualised. The signal tags (red) are from the classical PD signal. Because the switch signal is not in a related frequency to the interference signal the PD signal has not the same starting phase. A slightly pattern is visible in the unsorted matrix (a). In order to calculate the phase shift the time tags has to be shifted to the same starting phase position. The time tags shown in figure (b) are the result of individual shifts, which are applied to every single row. To achieve a higher accuracy the shift is made with float numbers.

First, to be able to shift the time tags to the same phase position (see Fig. 15b) the period of the signal has to be determined. Therefore the difference between the time tags is calculated. Sometimes for incomprehensible reasons the time-tagger misses a trigger signal. To avoid wrong differences a range was defined which only allows differences between a well defined range around the period time. To shift the single rows to the same phase position the single positions of the time tags are determined. Then using the period time and the modulo function an average shift for the single rows are calculated. Thereby sometimes if the time tags are settled around a multiple of the periode, a completely wrong shift was calculated. It is cause by time tags, which are sometimes settled at a position which is more or less than the periode. This periodic issue can be solved by a query, which calculate the standard deviation. Although, the row was only shifted if the standard deviation was smaller than the half of the period. Finally the time-tags are shifted by the amount of the checked shift. This steps is done for every row in the matrix. Next the time tags in the matrix after the phase shift have to be shifted by the same

amount to avoid to change the relation between matrices. Therefore, the shift of the n row in the prior matrix is used to shift the n row of the matrix after the phase shift.

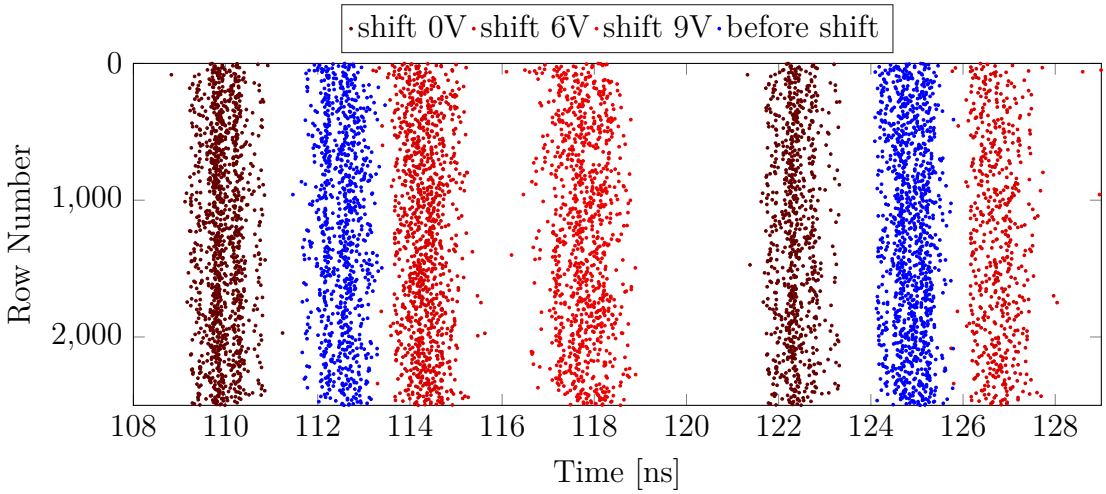

Figure 16: This diagram shows a scatter plot of the time tags. Thereby the y axis is describe the rows and the x axis the time. The time tags before the shift (blue) are all positioned on a similar position which confirms the sorting. However, the zero Volt measurement tag line has moved despite there is no electric field for a phase shift attached. Hence, the phase shift is not longer the different between the before time tags compared to the measurement time tags after the shift. The zero Volt measurement is used as the reverence phase shift for all later measurement with different voltages. Also, the different rising voltages produce rising phase shifts as already seen in classical oscilloscope measurement.

It seams that there is a negative phase shift (see Fig. 16). This may be explained by the pulse scheme of the measurement. The measurement with the time-tagger has two measurement pulses instead of one continuous measurement pulse. Consequently, the starting phase of the sinus between the measurement pulses of the PD signal can differ. This happens, when the time between the measurement pulses is not a multiple of the period time. The change of the phase in the presence of the electric field and the resulting phase shift are visible in figure 16. However, the difference between the prior matrix and the matrix after the shift is calculated. Afterwards the continuous shift, defined by the zero Volt measurement is removed.

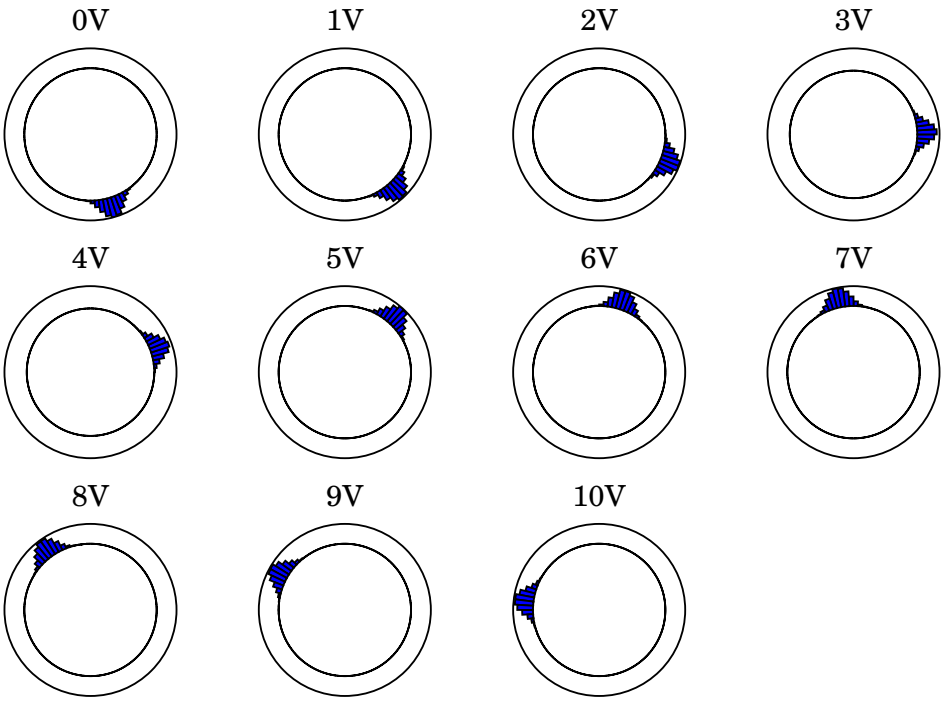

Figure 17: This graphic shows polar plots of the different shift related to their voltages. The blue histograms carrying the mean vectors of the matrices at a fixed voltage. A steady change of the angle of the histogram position is visible.

Another method is to map the position of the time tags of one row on a unit circle. Therefore the sorted even and odd number matrices are used. The following steps are executed for both matrices. First the x and y positions of the time tags on a unit circle are calculated by using trigonometrical functions and the period time. Then the means of the x and y positions for all time tags of a single row are determined. After this the position of the mean value of the prior matrix is traded as a vector and is rotated to the zero degree position of the unit circle. By applying the same rotation to the mean position of the vector, which describes the tags after the shift, the time tags are sorted similar as the previous method. The angle of this vector describe the phase of the shift. Ultimately, if this is calculated for all measurement voltages the angle of the zero Volt measurement has to be reduced from the other angles. The angle can be re-witten as a phase in units of π.

Both methods leads to highly similar results. The advantage of the unit circle mapping is, the independence of the missed time tags and the periodic issues of the time tag positions completely reduced.

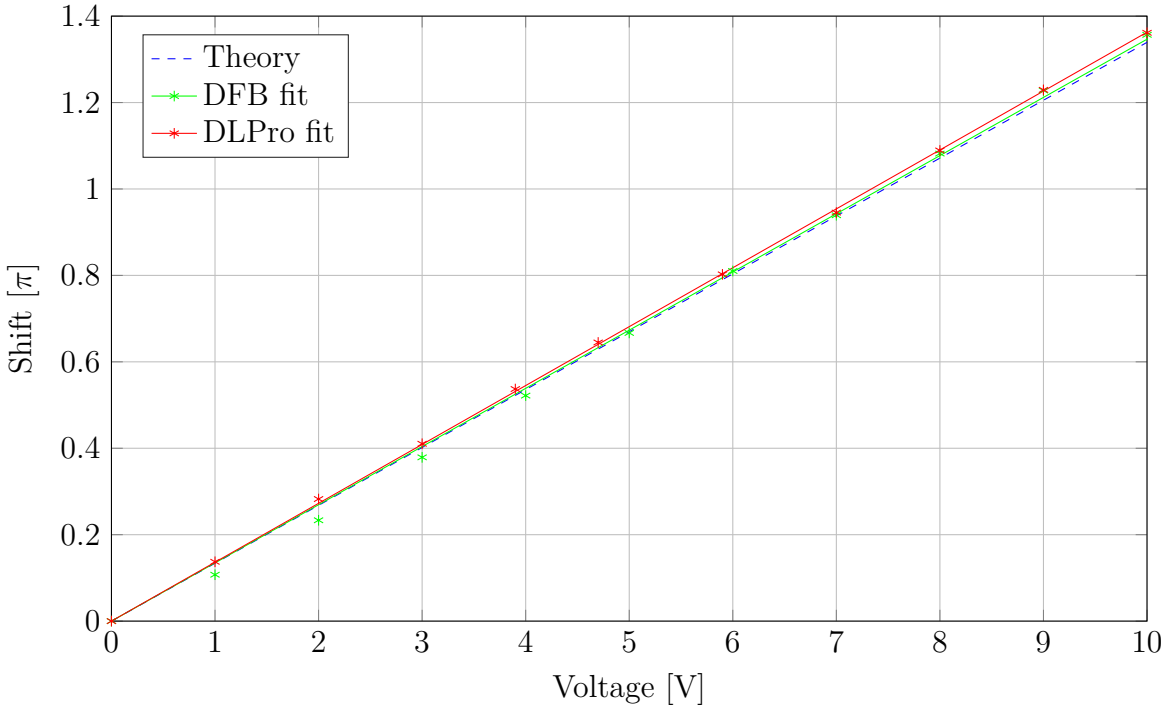

Figure 18: This diagram shows the phase shift in a unit of π in relation to the control voltage of the high voltage power supply. Sometimes inaccuracies of the single phase shifts at certain values of volt are visible. For this measurement the data of 150 matrices with 2500 rows are used.

The experimentally measured data can be compared with the theoretically calculated rise of the shift function. Therefore a linear function was fitted on the measured values. The result of the fit:

$$\Phi_{\text{DFB}}(V) = 0.1361 \pm 0.001 \cdot V \tag{3.21}$$

$$\Phi_{\text{DLPro}}(V) = 0.1359 \pm 0.001 \cdot V \tag{3.22}$$

$$\Phi_{\text{theory}}(V) = 0.1359 \cdot V \tag{3.23}$$

The linear fit functions don not differ much but by comparing the differences between the single measurements the oscilloscope measurement has a better linear behaviour of the data points, which fulfil the theory. Despite the inaccuracy of the single phase shift points the difference between the theoretically calculated rise of the function is less than 0.5%. This result shows, that only with one time tag per period an effective measurement of the phase shift can be made with the time-tagger. Nevertheless, the classical measurement using the oscilloscope only needs one measurement and less total measurement time per volt to achieve a better accuracy in comparison with the theoretic values.

4 Photon Measurement

4.1 Photon statistic

The classical theory of light is described by electromagnetic waves. The quantum theory of light consider the beam of light as a stream of photons. For the detection of a stream of photons a single photon counter module is used. The output amount of the photon counter depends on the photon flux Φ, which is the average number of the photons passing through a cross-section A of the beam in a unit time.[25] The photon flux can be calculated using the energy flux and the energy of the single photons:

$$\Phi = \frac{I \cdot A}{\hbar\omega} \equiv \frac{P}{\hbar\omega} \text{photons s}^{-1}, \tag{4.1}$$

where I is the intensity of the beam and P the power, which is the intensity in a specified area. Sometimes a photon counter detects incident photons. Therefore a photon counter has a specified quantum efficiency η which is the ratio of the number of photons over the incident photons. With the quantum efficiency the average number of counts in a counting time T is given by:

$$N(T) = \eta\Phi T = \frac{\eta P T}{\hbar\omega} \tag{4.2}$$

Thereby the average counting rate R in a second is given by:

$$R = \frac{N}{T} = \eta\Phi = \frac{\eta P}{\hbar\omega} \text{counts s}^{-1}. \tag{4.3}$$

With this equations the average photon numbers could be calculated. The distribution of coherent light with constant intensity has Poissonian photon statistic. In a beam segment of the length L corresponding to equation 4.3 the average number of photons $\overline{n}$ is given by:

$$\overline{n} = \frac{\Phi L}{c}, \tag{4.4}$$

where c is the physical constant of the speed of light. The probability $P(n)$ of finding n photons in a beam segment of the length L is given by:

$$P(n) = \frac{N!}{n!(N-n)!} \left(\frac{\overline{n}}{N}\right)^n \left(1 - \frac{\overline{n}}{N}\right)^{N-n}, \tag{4.5}$$

thereby the beam segment is divided into N subsegments. If we consider the number of subsegments N goes against infinity and by the use of the Sterling formula finally the photon statistic for a coherent light source can be described as[25]:

$$P(n) = \frac{\overline{n}^n}{n!} e^{-\overline{n}} \tag{4.6}$$

The statistic of light therefore is described with a Poisson distribution. A Possonian distribution is generally used to describe random processes that only return integer values. Thereby the distribution peak is at the position $\overline{n}$. The fluctuations of a statistical distribution about its mean value is quantified in terms of the variance. The variance correspond to the square of the standard deviation Δn.[25] In the case of a Poisson distribution the variance is defined by:

$$Var(n) \equiv (\Delta n)^2 = \sum_{n=0}^{\infty} (n - \overline{n})^2 P(n). \tag{4.7}$$

It also can be shown that that the variance is equal to the mean value $\overline{n}$, which means the standard deviation for the fluctuations of the photons is given by:

$$\Delta n = \sqrt{\overline{n}}. \tag{4.8}$$

Due to the fact that the photon counts have a Poisson distribution by measuring the photons some shot noise appears. This shot noise can be seen as the number of photons above and below the mean value of photon counts. Also a small amount is of the shot noise is related to the darkcounts of the photodiode. The noise can easily be described with the help of the photocurrent:

$$i = \eta e \Phi \equiv \eta e \frac{P}{\hbar \omega}, \tag{4.9}$$

where e is the modulus of the charge of the electron. The photocurrent $i(t)$ in relation to the time can be broken into a time-independent average current $< i >$ and a time varying fluctuation $\Delta i(t)$.

$$i(t) =< i > +\Delta i(t) \tag{4.10}$$

In average the value of $\Delta i(t)$ has to be zero, but not the square of Δi. For a precise measurement the photocurrent has to be higher than the noise of the signal. This derivation of photon statistic is based on the Oxford Master Series of Atomic, Optical,and Laser Physics from Mark Fox [25]. The proofs for the relations which are used in this chapter for example equation 4.8 can be found there.

4.1.1 Photon measurement

At the beginning of the measurement with the photoncounter the statistic of the laser light were investigated. Therefore the photon counter signal was measured with measurement pulses of 20 μs. Thereby a poissonian distribution was expected. With the theoretic mean count value of 51.5 photons per measurement pulse.

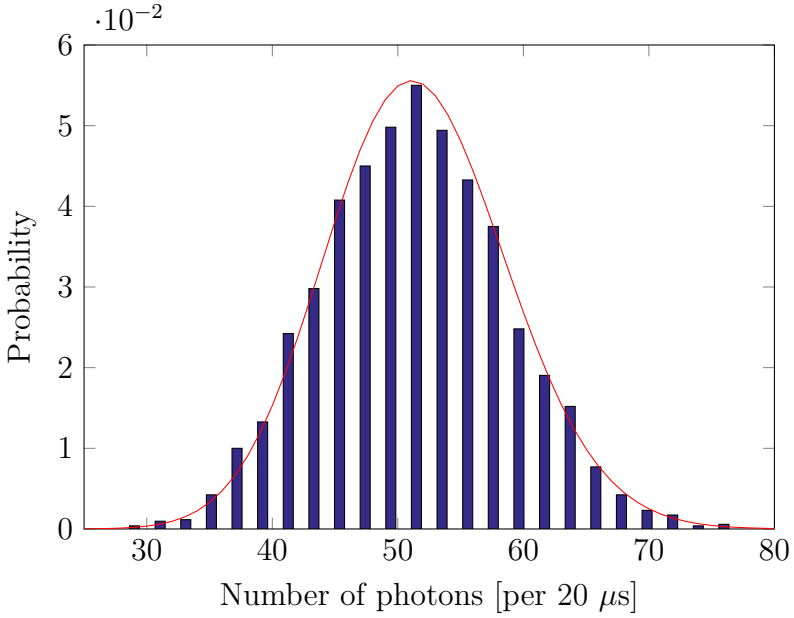

Figure 19: In this diagram a histogram of the photon counts per measurement pulse is plotted. For comparison, the theoretically calculated Poisson distribution of the theoretical mean count value is plotted (red).

The measurement data and the theoretically calculated distributions does not match perfectly. A possible reason for this inaccuracy may result from the dead time of the photon counter. However, the Poissonian statistic which is a prove for the coherent of the light can be verified with figure 19.

4.1.2 Phase shift measure at few photon level

For this measurement the pulse scheme from figure 14 is used to create the trigger signal for the time-tagger. The classical signal and the photon signal are measured at the same time. The photon time tags are saved in a 5000 x 2000 matrix as the classical signal. This matrix is also separated into a odd and even number matrix. To calculate a phase shift between the two matrices they have to be shifted to the same starting phase position like the classic matrices. Therefore the shift of the classical signal was used. The n row of the matrix with the classical tags correlate with the n row of the photon tag matrix. Every row is shifted by the same amount the rows of the classic matrix were shifted. After the shifting the matrices are summed over the columns. This procedure is necessary to receive a useful signal, because one single row of a matrix contains approximately only two photon tags. With this method for a time interval of 1000 ns the resulting signal contains 5000 photons. Moreover, the ratio of the shot noise compared to the actual signal is to high. Therefore, 150 matrices are measured of the same control voltage and summed together. Figure 20 shows the photon signal for a different amount of matrices. We expect to see a sharper sinus signal, which oscillate around the mean of the photon counts, with each added matrix.

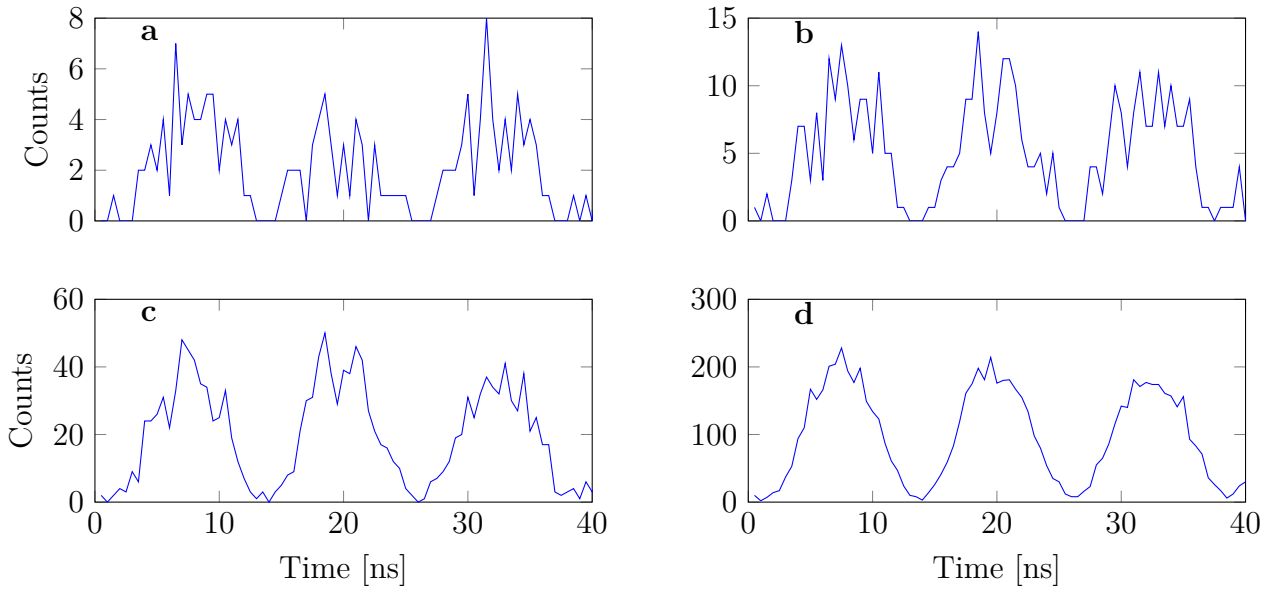

Figure 20: In this figure the dependency of the photon signal as a function of the amount of summed matrices is shown. Thereby figure (a) is only one matrix. With some imagination a barely sinus oscillation is visible. The shot noise of the signal is to high in comparison with the average number of photon tag per unit time. A sinus fit for this signal will have a huge inaccuracy. The ratio of the shot noise degrees with an increasing amount of matrices. This improvement of the signal is noticeable during the increase of matrices from figure (b) with five matrices, to figure (c) with 20 matrices to figure (d) with 100 matrices.

Figure 20 shows that the number of matrices which are used to calculate a photon signal is important. The measurement of one time tag matrix takes 5 s. To receive a good photon signal for the later calculation of the phase shift many matrices are necessary. To reduce the total measurement time the photons are shifted to the first periods, which leads to the same improvement as measuring more time tag matrices. Thereby, a modulo function is used to shift photons, which are not in the first periods into the first periods. A sinus fit needs some periods to reach its full accuracy. Therefore the accuracy as a function of periods are investigated. After eight periods no noticeable improvement of the accuracy could be made. Due to this conclusion the photons are shifted into the first eight periods..

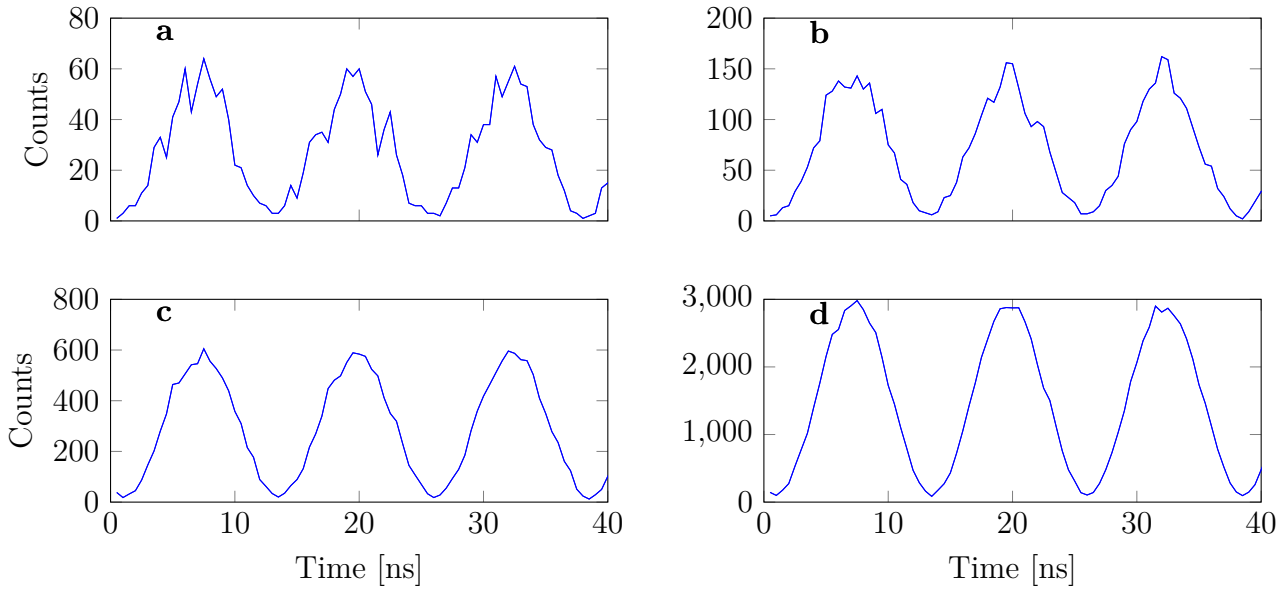

Figure 21: In this graphic the photons are shifted to the first eight periods. Figure (a) shows the measurement with one matrix. In the other figures more matrices are used:(b)=5, (c)=20 and (d)=100 matrices. In comparison with figure 20 a clear improvement is noticeable. With 5 matrices approximately the same results could be achieved like the 100 matrices in figure 20.

By the comparison of different amounts of matrices an improvement of more than ten times can be achieved. This improvement is described by the ratio between the amplitude and the shot noise.
The matrices have the same properties as the classic time tag matrix and therefore to deal with the same problem of two separated measurement pulses and different starting phases. Consequently, a similar method of analysis as it was used for the oscilloscope measurement is used. The only different is, that the fit areas are limited by the captured time of the matrices before and after the shift. Also the alignment measurement with a voltage of zero Volt is used as a reference phase shift. The other voltage measurements are related to this basic phase shift.

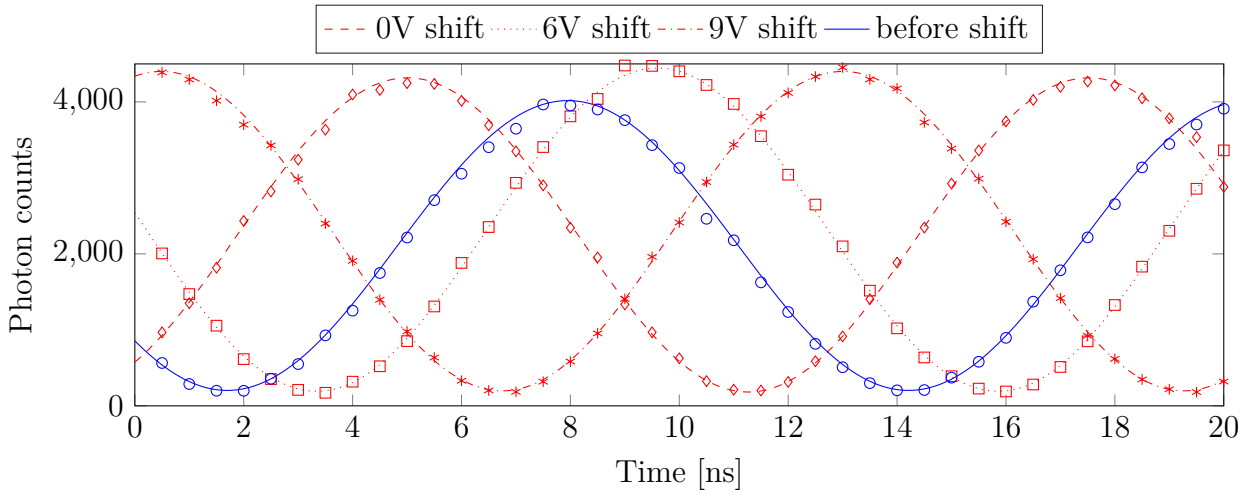

Figure 22: In this diagram the photon count signal fits are shown. The photon counts are plotted over the time. Hence, the measurement with a voltage of zero Volt is used to related all other measurement to it and calculate the relative phase shift of the different voltages. The phase shifts in the forward direction of the wave increases with rising voltage.

To calculate the relative phase shift the phase shifts are mapped on an unit circle. Therefore the x and y value of the phase shift was calculated using the standard trigonometrical functions cousins and sinus. We used a rotation matrix to rotate the before vector to the zero position of the circle. The vector which is the position after the shift was rotated by the same amount. A tangent function is used to calculate the angle of the position on the unit circle between 0 and 2π. The angular phase shift can be re-written in units of π. The last step is only to correct the shifts with the zero volt basic phase shift.

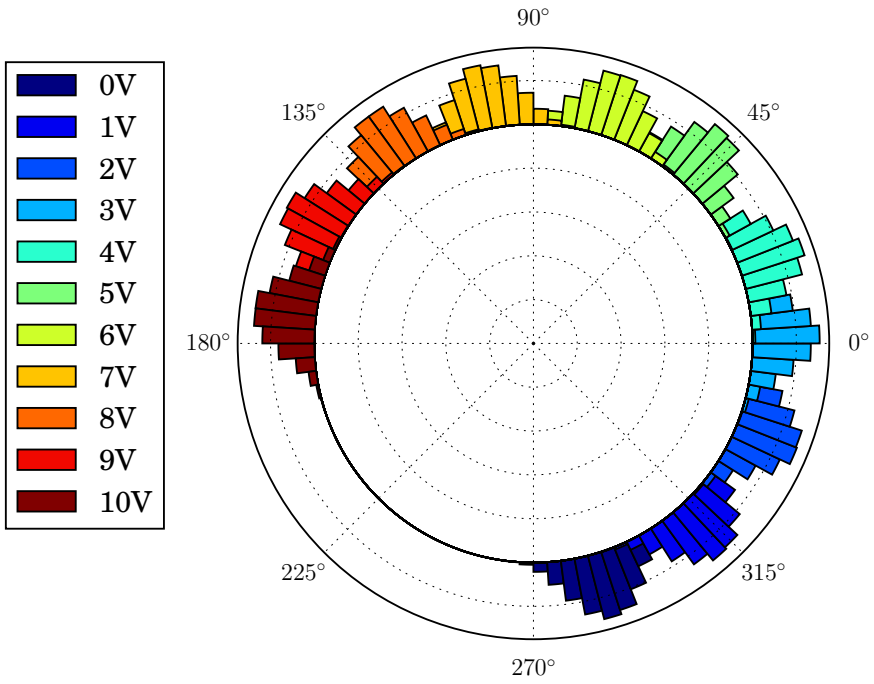

Figure 23: In this polar diagram the phases of the fit functions are mapped on a unit circle. Thereby, the histograms describe the phase with its inaccuracy (confidence bounds) of the different voltages. The positions of the rising voltages are steadily shifted anticlockwise.

With this method the relative phase shift of the photons can easily be calculated. The measurement is proved with a phase shift verification measurement using the DLPro laser. This leads to similar results which are visualised in figure 24. Thereby the function of the linear fits are:

$$\Phi_{\text{DFB}}(V) = 0.1348 \pm 0.0015 \cdot V, \tag{4.11}$$

$$\Phi_{\text{DLPro}}(V) = 0.1346 \pm 0.0015 \cdot V, \tag{4.12}$$

$$\Phi_{\text{theory}}(V) = 0.1359 \cdot V. \tag{4.13}$$

The calculated phase shifts have nearly the same phase shift as the theoretical ones. The theoretically calculated values are higher than the experimental measured ones. This behaviour was also observed in the classical measurements. The reason for this behaviour is tracked back to the inaccuracy of the HV power supply and some discontinuity. Small impurities in the crystal can lead to a lower phase shift with an unchanged linear behaviour.

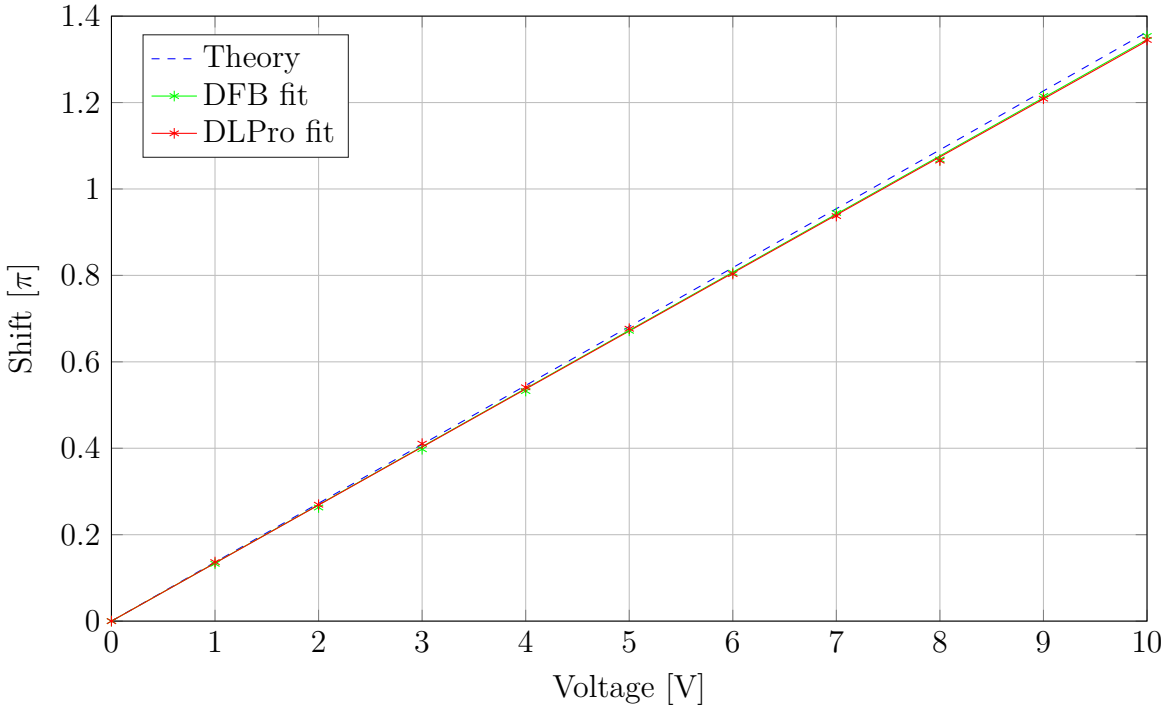

Figure 24: This figure shows the phase shift over the control voltage. To compare the measured phase shifts with the theoretic values, the theoretic function is plotted in this figure. A linear fit was made through the data of both lasers.

5 Error Analysis

In this experiment, errors are caused either by analysis or by devices with inaccuracy in the experimental setup. Moreover, the analysis method of a sinusoidal measurement signal, which uses two sinus fits to calculate the phase difference and the method which only saves time tags has to be considered separately.
To calculate the error caused by imprecise devices in the setup, the responsible devices have to be determined: the AOM, the EOM and the HV-supply.
The driver frequency of the AOM fluctuates at most $\pm 1\,\mathrm{kHz}$ over one hour. The error which occur to this inaccuracy was not calculated, because of its negligible small amount ($0.0001\ \pi$)
EOMs are very sensitive to disturbance of the electric field. For a determination of an error of the phase the theoretical values of phase shifts in dependency of voltage are calculated and compared with experimental measured values. This leads to an error parameter of 0.98 for the electric field.
The stability of the HV-supply was measured with an oscilloscope, which shows a noise oscillation with $\pm 5\,\mathrm{V}$.
With those assessments an additive error for due to the experimental setup becomes:

$$\Delta\Phi_{volt}(x) = 0.0136\pi, \tag{5.1}$$

$$\Delta\Phi_{efield}(x) = 0.002\pi \cdot x. \tag{5.2}$$

and therewith a total standard error of $\pm 0.0136\ \pi\ \pm 0.002 \cdot x$, thereby x describes the applied control voltage.
The error which is caused by the fit and analysis of the measured data occur due to the fit confidence bounds. By comparing the phase parameter prior and after the phase shift of the sinus fits, a minimum and maximum phase shift can be determined. This error is independent of the level of the control voltage only the sharpness of the signal is relevant. Therefore, an average error of the measurements with a sinus signal are calculated. The average inaccuracy of 0.003 in units of π is negligibly small.
For the classical signal measured with the time-tagger there is an error due to the use of alternative methods to calculate the phase shift and the bin size of $0.5\,\mathrm{ns}$. The error was calculated by using the standard derivation of the histogram plots around the unit circle. This leads to an phase inaccuracy of $0.1\,\mathrm{n}s$ which is an error of $\pm\ 0.012\ \pi$.
The larger inaccuracy of the of the classical sinus analysis (see Fig. 13) and the classical time-tagger analysis (see Fig. 18) is recognisable with the naked eye.
The results can be improved with the use of a preciser HV-switch, with less overshooting. Moreover, the measurement using the FPGA time-tagger of the classical signal can be realised with a smaller bin size. This was impossible in this bachelor thesis because smaller bin sizes on the same measurement time exceeded the matrix dimension which are permissible on a 32-bit system.

6 Conclusion and Outlook

The goal of this bachelor thesis was to build and characterise a setup for the measurement of a phase shift on a single-photon level. For this purpose, an optical setup was realised (see Fig.1). To verify the source independence of the setup two different lasers were used for the measurements. The phase shift was produced with a self-built EOM and then first measured using a classical signal from an AC photodiode. This measurement is used as a reference for the single-photon method utilising a SPCM.
Furthermore, the classical signal output of the AC photodiode was measured with an oscilloscope and with a FPGA based time-tagger. The motivation is to finally use only one analysing device (FPGA time-tagger) to determine the classical phase shift on a single-photon level. However, the classical measurement was first using carried out an oscilloscope and subsequently two sinusoidal fits, one prior and one after the phase shift to analyse the phase change. As a second approach the classical signal was measured with an FPGA time-tagger. This measurement methods saves time tag of the classical signal, whenever the classical sinusoidal signal passes a given trigger level. The time tags are then saved in a matrix (number of shot) x (number of bins). To measure prior and after the phase shift, two measurement pulses are used. These two measurement pulses are defined as one set of measurements and divided into two matrices (prior-, after-shift). The time between the different set measurements is not a multiple of the photodiode sinus signal. Consequently, the starting phase of the sinusoidal signal in the different sets differ and has to be shifted by the use of a modulo function to the same starting position (illustrated in Fig.15). Subsequently, the mean position of the single time tags are calculated by the use of the modulo function. This is carried out for the prior and after matrix. The differ of the mean modulo result may be re-written as a shift. Another method is to map the position of the time tags on a unit circle. By rotating the mean vector of the prior measurement to the zero position of the unit circle and applying the same rotation to the mean position of the vector, describing the tags after the shift, will sort all classical time tag measurements (see Fig.17). The angle of the different voltages describes the phase shift.
The measurement at a single-photon level using a SPCM is realised with the same measurement pulses at once (see pulse scheme Fig. 14). Hence the rotation of a set of classical tags can be re-written as a time shift. Therewith the related sets between the classical tags and the photon tag carrying matrix are shifted. After that the photons are summed vertically and shifted in the first eight periods two reach a higher signal per measurement. By the use of many matrices a clear sinusoidal signal appears which is used to fit a sine function. The comparison between the prior matrix fit phase and the after matrix fit phase determines the phase shift.
In summary, the values of the phase shift measured at a single-photon level can be verified with a classical measurement and a theoretic calculation. However, the classical light FPGA time tagger measurement has a higher inaccuracy than the classical oscilloscope measurement. A reason may be the bin size of the measurement which can be improved to a lower size. Nonetheless, the photon signal with the same bin size achieve higher precision, which probably can be traced back to the averaging and summing of the photons in the matrices.

This setup was developed to measure the phase shift of a light beam propagating through an atomic cloud. The phase shift is caused by the presence of a Rydberg atom in the cloud which, in turn, can be created using a single photon. A way to measure a phase shift difference produced by a Rydberg blockade uses an incoming beam of different polarised photons ($\sigma+$, $\sigma-$) [11]. Thereby the strong non-linear interaction between the $\sigma+$ photons can be detected. While the $\sigma-$ photons are used as a reference. With the exception of a not interfered polarised beam which is separately detected onto two SPCM the same setup and analysing algorithm can be used. With this additions the setup will be realised in the Rydberg experiment during the next year, to prove the phase shift of a light field with a single-photon transistor.

7 Acknowlegments

I would like to thank everybody who helped me during the creation of this thesis. In particular I want to thank:

- Prof. Dr. Tilman Pfau, for the opportunity of doing this thesis in the 5th institute.
- Dr. Sebastian Hofferberth, for being the supervisor of this thesis and always being there to answer questions and to help when needed. Including the whole RQO team A. Paris-Mondoki,I. Mirgorodskiy, C. Tresp, H. Gorniaczyk and Y. Zhou.
- Especially, I want to say thank you to my beloved girlfriend Ronja Müller. The relationship with her was motiviating me and gave me the strengh to work as hard as I could during this arduous time.
- At least I want to thank my partens, friends and family whose also supported me during this time.

Bibliography

[1] G.J. Milburn. "Quantum optical Fredkin gate". In: *Phys. Rev. Lett.* 52 (1989), pp. 2124–2127.

[2] I.L.Chuang M.A.Nielsen. *Quantum Computation and Quantum Information*. 1. Cambridge Univ. Pres, 2000.

[3] I.Fushman et al. "Controlled phase shifts with a single quantum dot". In: *Science* 320 (2008), pp. 269–772.

[4] Q.A.Turchette et al. "Measurement of conditional phase shifts for quantum logic". In: *Phys. Rev. Lett.* 75 (1995), pp. 4710–4713.

[5] V.Parigia et al. "Observation and measurement of interaction-induced dispersive optical nonlinea-rities in an ensemble of cold Rydberg atoms". In: *Phys. Rev. Lett.* 109 (2012), p. 233602.

[6] Lo et al. "Electromagnetically-induced-transparency-based cross-phase-modulation at attojoule levels". In: *Physical Review A - Atomic, Molecular, and Optical Physics* 83 (2011), pp. 3–6.

[7] A. K. Mohapatra, T. R. Jackson, and C. S. Adams. "Coherent Optical Detection of Highly Excited Rydberg States Using Electromagnetically Induced Transparency". In: *Phys. Rev. Lett.* 98 (11 Mar. 2007), p. 113003. DOI: 10.1103/PhysRevLett.98.113003. URL: http://link.aps.org/doi/10.1103/PhysRevLett.98.113003.

[8] Alexey V. Gorshkov et al. "Photon-Photon Interactions via Rydberg Blockade". In: *Phys. Rev. Lett.* 107 (13 Sept. 2011), p. 133602. DOI: 10.1103/PhysRevLett.107.133602. URL: http://link.aps.org/doi/10.1103/PhysRevLett.107.133602.

[9] H. Gorniaczyk et al. "Single-Photon Transistor Mediated by Interstate Rydberg Interactions". In: *Phys. Rev. Lett.* 113 (5 July 2014), p. 053601. DOI: 10.1103/PhysRevLett.113.053601. URL: http://link.aps.org/doi/10.1103/PhysRevLett.113.053601.

[10] Jürgen Volz et al. "Nonlinear π phase shift for single fibre-guided photons interacting with a single resonator-enhanced atom". In: *Nature Photonics* 8.12 (2014), pp. 965–970. URL: http://arxiv.org/abs/1403.1860$%5Cbackslash$nhttp://www.nature.com/doifinder/10.1038/nphoton.2014.253.

[11] Ofer Firstenberg et al. "Attractive photons in a quantum nonlinear medium." In: *Nature* 502.7469 (2013), pp. 71–75. URL: http://www.ncbi.nlm.nih.gov/pubmed/24067613$%5Cbackslash$nhttp://dx.doi.org/10.1038/nature12512$%5Cbackslash$n10.1038/nature12512$%5Cbackslash$nhttp://www.nature.com/nature/journal/v502/n7469/abs/nature12512.html%7B%5C#%7Dsupplementary-information$%5Cbackslash$nhttp://www.nature.com/doifinder/10.1038/nature12512.

[12] Jeffrey H. Shapiro. "Single-photon Kerr nonlinearities do not help quantum computation". In: *Phys. Rev. A* 73 (6 June 2006), p. 062305. DOI: 10.1103/PhysRevA.73.062305. URL: http://link.aps.org/doi/10.1103/PhysRevA.73.062305.

[13] Julio Gea-Banacloche. "Impossibility of large phase shifts via the giant Kerr effect with single-photon wave packets". In: *Physical Review A - Atomic, Molecular, and Optical Physics* 81.4 (2010). DOI: 10.1103/PhysRevA.81.043823.

[14] Kristin M. Beck et al. "Large conditional single-photon cross-phase modulation". In: *arXiv:1512.02166* (2015), p. 22. URL: http://arxiv.org/abs/1512.02166.

[15] Daniel Tiarks et al. "Optical Pi Phase Shift Created with a Single-Photon Pulse". In: (2015), pp. 1–14. DOI: 10.1126/sciadv.1600036. URL: http://arxiv.org/abs/1512.05740.

[16] Toptica. *toptica tunable diode laser*. 2016. URL: http://www.toptica.com/fileadmin/user%5C_upload/Brochures/toptica%20%5C_BR%5C_Tunable%5C_Diode%5C_Lasers.pdf.

[17] Dr. Michael Bass. *Handbook of Optiks II*. 3. Mc-Graw-Hill Companies, 2010. ISBN: 9780071629270.

[18] Dr. Rüdiger Paschotta. *Electro-optic Modulator*. 2016. URL: https://www.rp-photonics.com/electro_optic_modulators.html.

[20] Wolfgang Demtröder. *Experimentalphysik 2-Elektrizität und Optik*. 6. Springer-Verlag Berlin Heidelberg, 2013. ISBN: 9783642299445.

[19] Robert W. Boyd. *Nonlinear Optics*. 2. Elsevier Inc, 1992. ISBN: 9780121216825.

[21] Linbo, Mgo Niobate, Lithium Linbo, Crystal. *Lithium Niobate Crystal Series*. 2013. URL: http://www.lambdaphoto.co.uk/pdfs/Inrad_datasheet_LNB.pdf.

[22] CGC instruments. *NIM-AMX500-3 Bedienungsanleitung*. 2016. URL: http://www.cgc-instruments.com/data/Products/NIM/NIM-AMX500-3/Beschreibung-2.30_A.pdf.

[23] P. Hariharan. *Basics of Interferometry*. 2. Elsevier Inc., 2007. ISBN: 9780123735898.

[24] excelitas. *DTS_SPCM-AQRH*. 2016. URL: http://www.excelitas.com/downloads/DTS_SPCM-AQRH.pdf.

[25] Mark Fox. *Quantum Optics - An Introduction*. 2. Oxford Master Series in Atomic, Optical, and Laser Physics, 2005. ISBN: 9780198566724.